Title

HEAVY ION INDUCED SINGLE-NUCLEON TRANSFER REACTIONS IN THE Zr-Mo REGION

Authors

Zisman, M.S.
Becchetti, F.D.
Harvey, B.G.
et al.

Publication Date

1973-04-01

Submitted to Physical Review C

LBL-1676
Preprint

C. 1

HEAVY ION INDUCED SINGLE-NUCLEON TRANSFER REACTIONS IN THE Zr-Mo REGION

M. S. Zisman, F. D. Becchetti, B. G. Harvey,
D. G. Kovar, J. Mahoney, and J. D. Sherman

April 1973

Prepared for the U.S. Atomic Energy Commission
under Contract W-7405-ENG-48

LBL-1676

DISCLAIMER

LBL-1676

HEAVY ION INDUCED SINGLE-NUCLEON TRANSFER REACTIONS IN THE Zr-Mo REGION*

M. S. Zisman†, F. D. Becchetti, B. G. Harvey, D. G. Kovar, J. Mahoney and J. D. Sherman

Lawrence Berkeley Laboratory
University of California
Berkeley, California 94720

April 1973

ABSTRACT

The (^{16}O,^{15}N) and (^{16}O,^{15}O) reactions of targets of $^{90,91,94}Zr$, ^{92}Mo, and ^{93}Nb have been investigated with a 104 MeV ^{16}O beam from the Berkeley 88-inch cyclotron. Spectra for the (^{16}O,^{17}O) reaction (leading to the ground states of $^{90,93}Zr$) and for the (^{12}C,^{11}B) reaction on ^{90}Zr and ^{92}Mo at 78 MeV were also obtained. Outgoing heavy ions were detected in the focal plane of a magnetic spectrometer with a Borkowski-Kopp type position-sensitive proportional counter backed by a plastic scintillator. The (^{16}O,^{15}N) and (^{16}O,^{15}O) data indicate a preference for high angular momentum transfer similar to (but less pronounced than) that shown by the (α,t) and (α,^{3}He) reactions on the same targets. No evidence for a multi-step excitation of core-excited states is apparent from the present data.

I. INTRODUCTION

There is presently a great deal of interest in the spectroscopic information obtainable from heavy ion induced transfer reactions.[1] In particular, the (^{16}O,^{15}N) reaction at 60 MeV on all of the even Zr isotopes has been reported by Nickles et al.[2] The Zr-Mo region is a suitable choice for such a study since there are plentiful data from light ion reactions with which to compare. The (^{16}O,^{15}N) experiment of Nickles et al. was observed to strongly favor the capture of a $g_{9/2}$ proton by an undisturbed Zr core and indicated a preference for large angular momentum transfer similar to that shown by the (α,t) reaction on the same targets.[3,4] This preference can be understood qualitatively by estimating the favored momentum transfer for the heavy ion reaction as described by von Oertzen.[5] The results of this calculation,[6] summarized in Table I, indicate that at the grazing angle the (^{16}O,^{15}N) reaction has a favored momentum transfer $L \approx 3$. Similar calculations for the (α,t) reaction at 50 MeV and the (^{3}He,d) reaction at 31 MeV (also at the grazing angle) give favored momentum transfers of 4 and 0, respectively.

The Zr(^{16}O,^{15}N) results[2] were compared with the (^{3}He,d) results of Cates, Ball, and Newman[7] in order to determine which levels were populated by single-particle transitions. Several other states, not seen in (^{3}He,d), were interpreted[2] as possible core-excited levels of the type [Zr(2^+) ⊗ $\pi g_{9/2}$] or [Zr(3^-) ⊗ $\pi g_{9/2}$]. Observation of such states in (^{16}O,^{15}N) and not in (^{3}He,d) is, of course, very interesting, since it implies the existence of a multi-step reaction mechanism in this mass region which is specific to heavy ion reactions. At the present time the data of Nickles et al. provide the only evidence for such a multi-step reaction mechanism. The (^{16}O,^{15}N) data in the fp-shell do not indicate an important contribution from two-step processes,[8] nor do the

higher energy $^{208}Pb(^{16}O,^{15}N)$ data of Kovar et al.[9] However, essentially all of the proposed core-excited levels seen in the heavy ion experiment of Nickles et al.[2] were also visible in the (α,t) reaction[3,4] on these targets. To see whether this similarity of the $(^{16}O,^{15}N)$ and (α,t) reactions persisted at an ^{16}O energy somewhat further above the Coulomb barrier, spectra of the $(^{16}O,^{15}N)$ reaction were obtained on targets of $^{90,91,94}Zr$, ^{92}Mo, and ^{93}Nb at a beam energy of 104 MeV. Data on the neutron transfer reactions $(^{16}O,^{15}O)$ and $(^{16}O,^{17}O)$ were obtained simultaneously. Spectra from the $^{90}Zr(^{12}C,^{11}B)$ and $^{92}Mo(^{12}C,^{11}B)$ reactions at 78 MeV were also obtained in a separate experiment. Since the angular distributions of all the states seen in the heavy ion data were expected[10] to be similar, angular distributions were obtained only for the ^{90}Zr target. For the other targets spectra were taken near the expected maximum of the angular distribution.

II. EXPERIMENTAL

The experiments reported here were performed with 104 MeV $^{16}O(4+)$ and 78 MeV $^{12}C(3+)$ beams from the Berkeley 88-in. cyclotron, with typical currents of fully stripped ions of 100-500 nA on target. The targets used here were the same as those listed in Ref. 4, with two exceptions: A natural ^{93}Nb target, 150 μg/cm^2, was used in the heavy ion work and a new, thinner ^{92}Mo target, 150 μg/cm^2 (having the same isotopic composition as that listed in Ref. 4) was also employed.

Since the spectrometer and heavy ion detector are new, they will be described below briefly.

A. Spectrometer

A schematic diagram of the spectrometer[11] and 24-in. scattering chamber is shown in Fig. 1. The spectrometer is of the uniform field type with

quadrupole and sextupole lenses added for vertical focusing and aberration compensation. The spectrometer is dispersion-matched to the beam analyzing system.[12] Several features make this type of spectrometer well suited for heavy ion experiments: First, the particle orbits are isochronous to about 1% at the full solid angle (2 msr), which allows accurate time-of-flight measurements. As will be discussed below (Sec. II-C), this is essential for good mass separation. Second, the angle of incidence on the focal plane (90 ± 10°) and large dispersion (60 cm for $\Delta E/E$ = 30%) allow the use of a position-sensitive proportional counter without a significant loss of energy resolution. Further details of the spectrometer system may be found in Refs. 6 and 11.

B. Detector and Electronics

The position-sensitive detector used in the focal plane of the spectrometer is of the Borkowski-Kopp design.[13] It consists of a proportional counter 1 cm deep with anodes made from high-resistance carbon coated quartz wires.[14] The counter consists of 6 wires, 45 cm long, mounted horizontally in the focal plane with a vertical separation of 1 cm. The detector is mounted on a movable table with a bellows connecting it to the spectrometer vacuum chamber (see Fig. 1). For these experiments, the proportional counter was run at 620 V with a mixture of 93% Ar and 7% CH_4 at a pressure of 0.2 atm. Details of the construction of the counter used here may be found in Ref. 15. Similar devices are described in Refs. 16 and 17.

A simplified electronics block diagram is shown in Fig. 2. The electronic logic (see Ref. 15) is basically straightforward, although complications arise due to the widely different timing of the four signals (which must all arrive at the computer simultaneously). The right and left preamp signals from the proportional counter are used both for position and $\Delta E/\Delta X$ information.

The position information comes from a measurement of the risetime difference between the signals at the two ends of a wire.[13] Typical energy resolution for the (^{16}O,^{15}N) data was about 200 keV ($\Delta E/E = 0.2\%$). The $\Delta E/\Delta X$ signal is obtained by summing the right and left preamp outputs and then shaping the signal in an amplifier with a 16 μs peaking time. The purpose of the long time-constant is to obtain a signal which is essentially independent of position. Typical $\Delta E/\Delta X$ resolution in these experiments was about 10%.

The anode signal from the phototube is used for a time-of-flight (TOF) measurement with respect to the cyclotron rf. The resolution of the TOF signal is very dependent on cyclotron tuning, but was generally about 5 ns in these experiments. The signal from the last dynode of the phototube, while stored in the computer, was not utilized for particle identification. The response of the plastic scintillator is roughly linear with energy,[18] but the resolution obtained for ^{16}O ions ($\gtrsim$ 20%) was insufficient to resolve different peaks in the spectrum.

During a run, data are taken on-line by an SCC-660 computer and written on magnetic tape for final data analysis. At the same time, singles spectra of position, TOF, $\Delta E/\Delta X$, and dynode pulse height, and two-dimensional spectra of dynode signal vs position, TOF vs position, $\Delta E/\Delta X$ vs position, and TOF vs $\Delta E/\Delta X$ are accumulated and can be individually displayed on a storage scope. Sample two-dimensional spectra are shown in Figs. 3 and 4. Position spectra of the 6 individual wires are also stored in the computer.

C. Particle Identification

Data analysis of the heavy ion experiments is done off-line on the SCC-660 computer by replaying the data tapes obtained during a run. The TOF and $\Delta E/\Delta X$ signals are corrected for position dependence in order to set particle

gates.[15] A corrected TOF vs position spectrum is shown in Fig. 3.

Measurement of the four signals (position, TOF, $\Delta E/\Delta X$, dynode) makes it possible, at least in principle, to completely specify the identity of a heavy ion. However, three of these pieces of information (the dynode signal has insufficient resolution to be useful) are generally enough for particle identification. The identification scheme relies on two-dimensional plots of the various parameters. Non-relativistically we have

$$\text{Position} \propto B\rho \propto \frac{MV}{q} \tag{1}$$

$$\text{TOF} \propto \frac{1}{V} \tag{2}$$

and

$$\Delta E/\Delta X \propto Z^2\left(\frac{M}{E}\right)^n \propto \frac{Z^2}{V^{2n}} \tag{3}$$

where, for heavy ions in this energy range, $n \approx 1/2$. Thus, a plot of TOF vs position gives bands of particles corresponding to different values of M/q (see Fig. 3) and a plot of $\Delta E/\Delta X$ vs position (Fig. 4) separates particles according to Z^2. A TOF vs $\Delta E/\Delta X$ plot (Fig. 5) then allows one to set gates for different particle types. After gating, position spectra for the individual wires are merged using a calibration obtained either with an alpha source or by sweeping an elastic peak across the detector.

D. Cross Sections

Cross sections are obtained from the merged spectra as ratios to the elastic scattering cross section at the same angle, using a short "normalization" run. A separate normalization of the elastic scattering runs yielded

data in good agreement with optical model calculations. The normalizations were based on a monitor counter located in the scattering chamber.

In calculating cross sections it is necessary to know the relative charge state intensities of the heavy ions. During this experiment the ratio $^{16}O(8+)/^{16}O(7+)$ was measured on one target (^{93}Nb) and the ratio $^{15}O(8+)/^{15}O(7+)$ was obtained for ^{93}Nb, ^{92}Mo, and ^{90}Zr. (The $^{15}N(7+)/^{15}N(6+)$ ratio was not directly measured.) The results of these measurements agree well with the simple expressions given by Northcliffe:[19]

$$\varepsilon = 137\ \beta/Z = 137\ V/cZ \tag{4a}$$

$$R_{Z/Z-1} = 0.365\ \varepsilon^{4} \qquad (\varepsilon \lesssim 2) \tag{4b}$$

$$= 0.3\ \ \varepsilon^{4.35} \qquad (\varepsilon \gtrsim 2)$$

where V is the ion velocity and Z is its atomic number.

If $d\sigma_u$ are the "uncorrected" cross sections for the (^{16}O,^{15}N) and (^{16}O,^{15}O) reactions, calculated by ignoring charge state corrections in both the normalization and data runs, then the corrected cross sections are

$$d\sigma(^{15}N) = \frac{\chi(^{16}O)}{\chi(^{15}N)}\, d\sigma_u(^{15}N) \tag{5a}$$

and

$$d\sigma(^{15}O) = \frac{\chi(^{16}O)}{\chi(^{15}O)}\, d\sigma_u(^{15}O) \tag{5b}$$

where χ is the fraction of particles in the highest charge state. For heavy ions of the velocities encountered here,

$$\chi \approx \frac{R_{Z/Z-1}}{1 + R_{Z/Z-1}} \tag{6}$$

since the probability for a charge state Z-2 is less than 1%. From Eq. (4b) one gets (for an equilibrium charge distribution)

$$R_{8/7}(^{16}O) = 1.04\ R_{8/7}(^{15}O) \tag{7a}$$

and

$$R_{7/6}(^{15}N) = 1.89\ R_{8/7}(^{15}O). \tag{7b}$$

Assuming Eqs. (7a) and (7b) are valid for all targets then gives

$$d\sigma(^{15}N) = 0.94\ d\sigma_u(^{15}N) \tag{8a}$$

and

$$d\sigma(^{15}O) = d\sigma_u(^{15}O). \tag{8b}$$

The heavy ion cross sections reported in this paper have all been corrected in this manner. As long as only the fully stripped charge state is measured, this method leaves only a negligible uncertainty in the cross sections.

E. Position Calibration

For the ^{16}O experiment an internal calibration for each run was found by using various known peaks to obtain ρ as a function of channel number. The known ρ's were calculated using the measured average spectrometer field. These values for ρ were then fit by a least-squares program,[20] which generated a quadratic calibration curve from which the magnetic rigidities of unknown peaks were obtained. This procedure is not highly accurate, so the excitation energies quoted here for ^{16}O induced reactions generally have rather large uncertainties. For the ^{12}C experiment the calibration curve was obtained by sweeping elastically scattered particles across the focal plane detector.

III. RESULTS

A. Selection Rules

The selection rules for heavy ion induced single-nucleon transfer reactions have been obtained by several authors within the DWBA framework.[21,22]

They are:

$$\ell_1 + \ell_2 \geq L \geq |\ell_1 - \ell_2| \tag{9}$$

$$j_1 + j_2 \geq L \geq |j_1 - j_2| \tag{10}$$

and

$$\ell_1 + \ell_2 + L = \text{even} \tag{11}$$

where ℓ_1, j_1 and ℓ_2, j_2 are the orbital and total angular momenta of the captured nucleon in the projectile and final nucleus, respectively, and L is the transferred angular momentum. For both the $(^{16}O, ^{15}N)$ and $(^{16}O, ^{15}O)$ reactions studied here $\ell_1 = 1$ and $j_1 = 1/2$ (i.e., the transferred nucleon in the projectile is in a $1p_{1/2}$ state), and Eqs. (9) to (11) require

$$L = \ell_2 + 1 \qquad \text{for } j_2 = \ell_2 + 1/2 \tag{12a}$$

and

$$L = \ell_2 - 1 \qquad \text{for } j_2 = \ell_2 - 1/2. \tag{12b}$$

For the $(^{12}C, ^{11}B)$ reaction, where $\ell_1 = 1$ and $j_1 = 3/2$, the selection rules allow

$$L = \ell_2 \pm 1 \qquad \text{for } j_2 = \ell_2 + 1 \text{ and } j_2 = \ell_2 - 1 \tag{13}$$

(except for $j_2 = 1/2$). Thus, one expects to see differences in the $(^{16}O, ^{15}N)$ and $(^{12}C, ^{11}B)$ spectra due to the different selection rules as well as due to kinematics.[9]

These results are in contrast with light ion selection rules where, because $\ell_1 = 0$, a single L value, $L = \ell_2$, is allowed for both $j_2 = \ell_2 + 1/2$ and $j_2 = \ell_2 - 1/2$ transfers. It has been pointed out[5] that the parity selection rule, Eq. (11), is only approximate since it results from ignoring recoil effects in obtaining the DWBA expression for the transition amplitude. Since

the predicted DWBA cross sections depend very strongly on L ($\sigma_{L+2} \approx 10\ \sigma_L$), an implication of the above selection rules is that a very strong j-dependence is expected in the ($^{16}O,^{15}N$) and ($^{16}O,^{15}O$) reactions. However, the experimental evidence[9] indicates a j-dependence which, although clearly visible, is considerably weaker than would be obtained from DWBA predictions. Apparently, this is due to the neglect of the recoil terms.[23] In any case, validity of the parity selection rule has not been thoroughly investigated.

B. $^{90}Zr(^{16}O,^{15}N)^{91}Nb$

A ^{15}N spectrum from the $^{90}Zr(^{16}O,^{15}N)^{91}Nb$ reaction at $\theta_\ell = 25°$ is shown in Fig. 6. The resolution is about 200 keV (FWHM). This reaction has been observed previously by Nickles et al.[2] at 60 MeV. Table II summarizes the states observed in this work and their intensities. Compared with those of Nickles et al.,[2] the cross sections are much larger (about a factor of 6) at the higher beam energy used here.

Angular distributions for the ground and 3.37 MeV states are shown in Fig. 7. Based on the selection rules (Sec. III-A) the ground state corresponds to an L = 5 transition while the 3.37 MeV $d_{5/2}$ state requires L = 3. It can be seen from Fig. 7 that the $^{90}Zr(^{16}O,^{15}N)$ reaction shows essentially no L-dependence in the angular distributions, in agreement with the results of other ($^{16}O,^{15}N$) studies.[2,24] The observed angular distributions can be understood in terms of a semi-classical picture even at energies much greater than the Coulomb barrier (which is about 39 MeV for the ^{16}O-^{90}Zr system). At backward angles (small impact parameters) the transfer cross sections decrease due to absorption, and at forward angles (large impact parameters) the cross sections decrease because the projectile and target nuclei are outside the range of the nuclear force which is responsible for the transfer. The peak of

the angular distribution comes near the grazing angle, where σ/σ_R deviates from unity. For these data the grazing angle is about 25° (lab). Also shown in Fig. 7 are the results of DWBA calculations, which are discussed in Sec. V.

In the low energy (^{16}O,^{15}N) data[2] the spectrum cuts off at about 4 MeV excitation energy due to the Coulomb barrier, so only states below 3.37 MeV can be compared. In both (^{16}O,^{15}N) experiments the ground and 3.37 MeV states are the strongest, with the ground state being stronger by a factor of 4 in these data and by a factor of 9 in the 60 MeV experiment. The weaker population of the 3.37 MeV state at 60 MeV might be due to the proximity of the ^{15}N to the Coulomb barrier. Near the 1.61 MeV state reported in Ref. 2, there are three states seen here, at 1.29, 1.60, and 1.88 MeV. The 2.18 MeV state reported by Nickles et al.,[2] whose intensity was somewhat larger than that of their 1.61 MeV state, does not appear here (see Fig. 6). This state and the state at 2.75 MeV were tentatively suggested to be core-excited states of the type $[^{90}Zr(2^+) \otimes \pi g_{9/2}]$ and $[^{90}Zr(3^-) \otimes \pi g_{9/2}]$, respectively, in Ref. 2,based mainly on their excitation energies. The 2.75 MeV state is also absent in the (^{16}O,^{15}N) data obtained here, unless it corresponds to the level at 2.97 MeV. A 200 keV error in the excitation energy of the 2.97 MeV level seen here is unlikely, however, since it is so close to the 3.37 MeV state which was used as a calibration point at all angles.

Above the 3.37 MeV state there are several levels seen in the $^{90}Zr(^{16}O,^{15}N)$ data which were not observed in the previous experiment. These states extend up to 6.6 MeV of excitation energy, above which no states were observed. The states at 5.9 and 6.6 MeV are very broad (see Fig. 6). This could be due to population of unbound states in ^{91}Nb at these energies but, since similar groups at high excitation energies appear in the

^{15}N spectra of the other targets studied, it seems reasonable to also consider the possibility of (Doppler broadened) ^{15}N excited states. Such "shadow peaks" have been observed in some heavy ion reactions,[25] but not in (^{16}O,^{15}N) specifically.

The first excited states of ^{15}N occur at 5.27 and 5.30 MeV. However, these are $5/2^+$ and $1/2^+$ levels and cannot be reached directly from the ^{16}O ground state except through admixtures of 2p-2h, etc., components. The third excited state in ^{15}N, at 6.33 MeV, is a $p_{3/2}^{-1}$ level and thus can be reached from the major (closed shell) component of the ^{16}O ground state. (The $^{16}O(d,^3He)^{15}N$ reaction,[26] for example, yields a cross section for the 5.27-5.30 MeV doublet about 10 times smaller than those for the ground and 6.33 MeV states.) Obviously neither of the observed excited states has exactly the right energy to be the 6.33 MeV state in ^{15}N, but the average of the two energies (6.25 MeV) agrees quite well.

A similar result was observed in the inelastic scattering data, which was obtained simultaneously with the (^{16}O,^{15}O) results reported below. In all of the inelastic ^{16}O spectra (Fig. 8) a broad doublet appears at excitation energies of 5.7 and 6.4 MeV. The appearance of these states at the same excitation energies and with the same cross sections (within about 20%) in the ^{90}Zr, ^{92}Mo, and ^{93}Nb targets suggests that a similar transition is involved. Here too, neither of the peaks corresponds in energy to an ^{16}O excited state, but the average energy, 6.05 MeV, could be explained by population of the 6.13 MeV 3^- state in ^{16}O. The 6.05 MeV 0^+ state in ^{16}O is unlikely to be populated by inelastic scattering since it is orthogonal to the ^{16}O ground state and is believed to be mainly a 4p-4h level.

The appearance of a double peak in these two cases could occur if the excited states are aligned with respect to the outgoing particle direction.

From the results obtained here it is not possible to unambiguously interpret the highest excited states in the ^{15}N spectrum. All that can be said is that the levels near 6 MeV are probably due to ^{15}N excited states.

C. $^{90}Zr(^{12}C,^{11}B)^{91}Nb$

A spectrum of the $^{90}Zr(^{12}C,^{11}B)^{91}Nb$ reaction at $\theta_\ell = 25°$ is shown in Fig. 6. A comparison of the $^{90}Zr(^{12}C,^{11}B)$ spectrum with that from the $^{90}Zr(^{16}O,^{15}N)$ reaction (also in Fig. 6) indicates a peak due to the ^{11}B $1p_{1/2}$ level at 2.124 MeV. As expected for a Doppler broadened level, the peak width of the ^{11}B 2.12 MeV state is about 300 keV or twice the experimental resolution. The absence of ^{91}Nb levels near 6 MeV in the ^{11}B spectrum indicates that the levels at this energy seen in the $^{90}Zr(^{16}O,^{15}N)$ data are due to a ^{15}N excited state, as discussed above (Sec. III-B). A summary of the levels observed in the $^{90}Zr(^{12}C,^{11}B)$ reaction and their intensities is included in Table II.

The relative increase in the population of the levels at 4.2 and 4.8 MeV in $(^{12}C,^{11}B)$ compared with $(^{16}O,^{15}N)$ suggests that these states have $j_2 = \ell_2 - 1/2$ or have high spin. The 4.8 MeV state has been seen in $^{90}Zr(^3He,d)$ and assigned[15] $\ell=4$ $(g_{7/2})$, in agreement with its strong population in $^{90}Zr(\alpha,t)$.[3] The 4.2 MeV level was also strongly populated in (α,t) although it was assigned[7] $\ell=2$ in $(^3He,d)$. Based on the arguments in Ref.3, the preferred shell model assignments for the 4.18 MeV state seen in $^{90}Zr(\alpha,t)$ are $9/2^+$, $7/2^+$, and $11/2^-$. If this state is the same as that populated in the $^{90}Zr(^{16}O,^{15}N)$ and $^{90}Zr(^{12}C,^{11}B)$ reactions, a $g_{7/2}$ or $h_{11/2}$ assignment is most reasonable. Certainly a comparison between the $(^{16}O,^{15}N)$ and $(^{12}C,^{11}B)$ data indicates that the 4.2 MeV state is not a $d_{5/2}$ fragment. This result is consistent with the DWBA calculations discussed below (Sec. V).

D. $^{92}Mo(^{16}O,^{15}N)^{93}Tc$

The $^{92}Mo(^{16}O,^{15}N)^{93}Tc$ reaction was studied only at θ_ℓ = 20 and 25°. As can be seen from Fig. 9, the spectra look very similar to those from the $^{90}Zr(^{16}O,^{15}N)^{91}Nb$ reaction (Fig. 6). A summary of the levels identified in the $^{92}Mo(^{16}O,^{15}N)$ reaction is given in Table III, along with the cross sections for the ground and 3.36 MeV states seen by Christensen et al.[27] at 66 MeV. As for the $^{90}Zr(^{16}O,^{15}N)$ data (Sec. III-B), the cross sections observed at 104 MeV are significantly larger than those reported at 66 MeV. The cross section ratio of the ground and 3.36 MeV states in ^{93}Tc is about the same as that observed for the corresponding ^{91}Nb levels. The low-lying $p_{1/2}$ state, at 0.39 MeV in ^{93}Tc, is resolved from the ground state in these data, and has a cross section about 1/6 of the latter. The 0.10 MeV $p_{1/2}$ state in ^{91}Nb was not resolved from the ground state in $^{90}Zr(^{16}O,^{15}N)$. Therefore, assuming the same relative strengths as in ^{93}Tc, the ^{91}Nb ground state cross section quoted in Table II is too large by about 15 to 20%.

Near 6 MeV in ^{93}Tc there are broad states in the ^{15}N spectrum similar to those found in $^{90}Zr(^{16}O,^{15}N)$. If the ^{91}Nb ground state cross section is corrected for the presence of the unresolved $p_{1/2}$ level, then the cross sections (relative to the ground states) of the 5.9 and 6.7 MeV states seen in the two reactions differ by less than 10%. This is consistent with the hypothesis that these states are due to excited ^{15}N levels.

E. $^{92}Mo(^{12}C,^{11}B)^{93}Tc$

A spectrum of the $^{92}Mo(^{12}C,^{11}B)^{93}Tc$ reaction at θ_ℓ = 25° is shown in Fig. 9. The ^{11}B 2.12 MeV peak is clearly visible and has an intensity relative to the ^{11}B ground state about the same as that found with the ^{90}Zr target. A summary of the levels observed and their intensities is included in Table III.

In agreement with the ^{90}Zr data, the 6 MeV levels in $^{92}Mo(^{16}O,^{15}N)$ do not appear in $^{92}Mo(^{12}C,^{11}B)$.

The relative enhancement of the ^{93}Tc 3.9 and 4.7 MeV levels in $(^{12}C,^{11}B)$ compared with $(^{16}O,^{15}N)$ suggests that these levels have $j_2 = \ell_2 - 1/2$. Strong levels near these energies were observed in the $^{92}Mo(\alpha,t)$ reaction,[3] which would be consistent with population of $g_{7/2}$ states in the heavy ion reactions. The results of DWBA calculations for these data will be discussed in Sec. V.

F. $^{94}Zr(^{16}O,^{15}N)^{95}Nb$

This reaction was observed at θ_ℓ = 25 and 30°. A summary of the levels observed here, compared with those seen in the 60 MeV $^{94}Zr(^{16}O,^{15}N)$ data of Nickles et al.,[2] is given in Table IV. A spectrum of the $^{94}Zr(^{16}O,^{15}N)^{95}Nb$ reaction at θ_ℓ = 25° is shown in Fig. 10. The resolution is 300 keV (FWHM). Here too the cross sections are larger than those observed in the 60 MeV experiment, although by much less than was true for the $^{90}Zr(^{16}O,^{15}N)$ data (see Sec. III-B). The strong low-lying states at 0.75, 1.6, and 2.05 MeV seen by Nickles et al.[2] are also the strongest states seen at 104 MeV. The cross section listed in Table IV for the $p_{1/2}$ state at 0.26 MeV was obtained from the Gaussian peak fitting program DERTAG.[28] The contribution of the upper level to the ground state peak is about 16%, in agreement with the ratio obtained from the (resolved) 0.39 MeV level in ^{93}Tc. Since the spectroscopic factors for the low-lying $p_{1/2}$ levels in ^{91}Nb, ^{93}Tc, and ^{95}Nb are all quite similar, a correction of about 15% to the ^{91}Nb ground state cross section listed in Table II would be a reasonable estimate.

At higher excitation energies there appear four broad groups in the ^{15}N spectrum (see Fig. 10). The upper groups, at 5.9 and 6.8 MeV, are similar to those seen in the $^{90}Zr(^{16}O,^{15}N)$ and $^{92}Mo(^{16}O,^{15}N)$ reactions and are probably

due to an ^{15}N excited state. The other two groups, at 3.8 and 4.8 MeV, must be ^{95}Nb levels since they are well below the first excited state in ^{15}N. However, with data at only two angles, it was not possible to obtain any meaningful information about individual levels in these groups. The energies and cross sections for these "states" refer to the whole multiplet, rather than to any single level, as is indicated by the arrows in Fig. 10.

G. $^{91}Zr(^{16}O,^{15}N)^{92}Nb$

The $^{91}Zr(^{16}O,^{15}N)^{92}Nb$ reaction was studied only at $\theta_\ell = 25°$. The spectrum is shown in Fig. 11. Since the target ground state has $J^\pi = 5/2^+$, each single-proton state forms a multiplet of levels. The $\pi g_{9/2}$ state, for example, forms a $(\pi g_{9/2}, \nu d_{5/2})_{2^+ \to 7^+}$ multiplet in ^{92}Nb which spans 500 keV of excitation energy.[29] As can be seen from Fig. 11, the largest peak has a centroid (0.4 MeV) and width ($\approx$ 500 keV FWHM) consistent with populating all the states of this multiplet. A summary of the levels observed in the $^{91}Zr(^{16}O,^{15}N)^{92}Nb$ reaction is given in Table V. A comparison of the cross section of the 0.4 MeV "state" in ^{92}Nb with that of the ground state of ^{91}Nb (Table II) indicates that about 90% of the $\pi g_{9/2}$ strength can be accounted for in this multiplet. This result agrees very well with the corresponding measurement made with the (α,t) reaction.[4] The other strong group in the spectrum, at 3.6 MeV, is expected to be a $[^{91}Nb(3.37\ MeV) \otimes \nu d_{5/2}]$ multiplet based on the observed strong population of the 3.37 MeV $\nu d_{5/2}$ state in the $^{90}Zr(^{16}O,^{15}N)^{91}Nb$ reaction (Sec. III-B).

At higher excitation energy a very broad group appears with a centroid energy of 6.3 MeV. This group does not look like the 6 MeV groups observed in the spectra of the even-even targets (see, for example, Fig. 6), since it is not a double peak. The centroid energy of the group, however, still agrees

well with the energy of the $p_{3/2}^{-1}$ excited state in ^{15}N. The difference in shape in this case may be due to the "valley" between the 5.9 and 6.6 MeV peaks in $^{90}Zr(^{16}O,^{15}N)$ being destroyed by averaging over the 500 keV wide ground state multiplet in ^{92}Nb. Also, since the level density of the odd-odd ^{92}Nb nucleus is undoubtedly greater than that of ^{91}Nb at the same excitation energy, there is probably more cross section in this region due to "real" ^{92}Nb states, which might have the effect of washing out the double peak structure.

H. $^{93}Nb(^{16}O,^{15}N)^{94}Mo$

The $^{93}Nb(^{16}O,^{15}N)^{94}Mo$ reaction was studied at θ_ℓ = 20 and 25°. The spectrum taken at θ_ℓ = 20° is shown in Fig. 12. The ground state and low-lying levels are populated rather weakly and the spectrum is dominated by a doublet at 2.6 and 2.9 MeV. Based on the $^{93}Nb(^{3}He,d)$ results of Cates, Ball, and Newman,[7] there are many ^{94}Mo levels in the region near 2.6 MeV. Spin assignments to some of these have been made by Lederer, Jaklevic, and Hollander[30] in a study of in-beam γ-ray spectroscopy of the even molybdenum isotopes. The γ-decay data[30] indicate levels at 2.421 MeV (6^+), 2.608 MeV (5^-), 2.738 MeV (4^+), 2.870 MeV (6^+ or 6^-), and 2.953 MeV (8^+ or 8^-). These last two levels are connected by an E2 decay and thus must have the same parity. The $^{93}Nb(^{3}He,d)$ reaction[7] assigns ℓ = 4 to the 2.875 and 2.960 MeV states, which suggests that these levels are the 6^+ and 8^+ of the $(\pi g_{9/2})^2$ configuration. Similarly, the strong ℓ = 1 transition to the 2.614 MeV level in $(^{3}He,d)$ indicates a dominant $(\pi p_{1/2}^{-1}\ g_{9/2})_{5^-}$ configuration for that state. A summary of the levels observed in the $^{93}Nb(^{16}O,^{15}N)$ reaction, as well as those seen in the $(^{3}He,d)$ and γ-decay experiments, is given in Table VI.

The highest state seen here, at 4.1 MeV, was not reported in Ref. 7.

A number of levels in this region were seen in the γ spectroscopy experiment and given high-spin assignments ($J \geq 8$). Such high-spin states are likely to be multiparticle states. The exceptions to this are the 9^- and 10^- states which arise from the $(\pi h_{11/2}\ g_{9/2})$ configuration. However, the $\pi h_{11/2}$ single-particle energy is quite high (> 6 MeV) in ^{93}Tc and is probably not too different in ^{94}Mo. The probable 10^+ state at 3.894 MeV, for example, was tentatively associated with the $[(\pi g_{9/2})^2_{8^+}(\nu d_{5/2})^2_{2^+}]$ configuration. In a single-step stripping reaction, such a level could only be reached through an admixture of $[(\pi g_{9/2})(\nu d_{5/2})^2_{2^+}]_{9/2^+}$ in the ^{93}Nb ground state. Another possible explanation for states in this region would be levels with a dominant $\pi d_{5/2}$ configuration. Such states would be expected at about this excitation energy. The $\ell = 2$ admixtures determined for the low-lying levels seen in ^{93}Nb(^{3}He,d) were all quite small, indicating that the major $\pi d_{5/2}$ strength does lie at higher energies.

At very high energies in ^{94}Mo very broad structures appear in the spectrum. The excitation energies of two of these "levels", 8.8 and 9.9 MeV, could correspond to the double excitation which gives ^{94}Mo (2.9 MeV) and ^{15}N (6.33 MeV), in agreement with previous evidence.

I. ^{90}Zr(^{16}O,^{15}O)^{91}Zr

A spectrum of the ^{90}Zr(^{16}O,^{15}O)^{91}Zr reaction at $\theta_\ell = 25°$ is shown in Fig. 13. The resolution is about 250 keV (FWHM). To facilitate later comparison, a spectrum of the ^{90}Zr(α,^{3}He)^{91}Zr reaction at 65 MeV is included. As can be seen from Fig. 13, only two levels are strongly populated, the ground and 2.16 MeV states. The angular distributions for these states, shown in Fig. 14, are quite similar to those from the ^{90}Zr(^{16}O,^{15}N)^{91}Nb reaction (Fig. 7). Both the ^{15}O and ^{15}N angular distributions peak at about the

same angle, but the ^{15}O angular distributions fall off more rapidly at forward angles than do those of ^{15}N.

The expected Q-value dependence of sub-Coulomb heavy-ion induced transfer reactions has been discussed by Buttle and Goldfarb.[31] They find that for neutron transfer the favored Q-value is zero. This is a consequence of requiring that the distance of closest approach be approximately the same in both the initial and final channels. In the case of the (^{16}O,^{15}N) reaction this requirement favors a negative Q-value since there is a change in the outgoing Coulomb barrier. For neutron transfer, a zero Q-value corresponds roughly to a momentum transfer of zero. In the present case, the ground state ($d_{5/2}$) transition requires L = 3 and the transition to the 2.16 MeV state ($h_{11/2}$) requires L = 6 according to the selection rules (Sec. III-A). From the kinematic model described in Refs. 5 and 6 an L = 3 transition corresponds to a Q-value of -1.5 MeV, while an L = 6 transition corresponds to a Q-value of -6 MeV. Thus, in this simple picture the ground state (L = 3) is about 7 MeV away from the favored Q-value and the 2.16 MeV state (L = 6) is off by about 4.5 MeV.

The Q-value dependence of heavy ion reaction cross sections is predicted to be quite steep.[31,32] Manko et al.[33] observed changes in cross section of about one order of magnitude for a Q-value change of 5 MeV in the (^{16}O,^{15}N) reaction on the nickel isotopes leading to the $\pi g_{9/2}$ states in copper. According to the calculations of Buttle and Goldfarb,[31] the Q-value dependence for neutron transfer is even more pronounced than for proton transfer and they suggested that it would be necessary to select a reaction whose Q-value was near the optimum value in order to obtain "measurable" cross sections for single nucleon transfer reactions. The data obtained here show cross sections

for the ground and 2.16 MeV states (whose Q-values are -8.5 and -10.6 MeV, respectively) of 3 mb/sr at $\theta_\ell = 25°$. This indicates that measurable cross sections are obtainable with the (^{16}O,^{15}O) reaction at high bombarding energies, even for very negative Q-values. Since conventional no-recoil DWBA calculations (see Sec. V) predict correctly the magnitude of the cross sections measured here, it seems apparent that the Q-value dependence at 104 MeV is less acute than suggested by the sub-Coulomb model of Buttle and Goldfarb.[31]

The levels of ^{91}Zr have been studied by means of the $^{90}Zr(d,p)^{91}Zr$ reaction.[34-36] The ground state is the $\nu d_{5/2}$ single-particle level and is observed with a spectroscopic factor of approximately unity in all cases. The situation for the doublet at 2.16 and 2.19 MeV is not so unambiguous since the two levels are assigned different ℓ values by the various groups. Cohen and Chubinsky[34] and Graue et al.[35] see only $\ell = 4$ strength, while Bingham and Halbert[36] and Booth et al.[37] assign the upper member as $\ell = 4$ ($g_{7/2}$) and the lower member as $\ell = 5$ ($h_{11/2}$). The $^{91}Zr(p,p')$ data of DuBard and Sheline[38] also give $J^\pi = 11/2^-$ for the 2.16 MeV state. Since the two levels were not resolved by Cohen and Chubinsky and the data of Graue et al. are fit equally well with either an $\ell = 4$ or an $\ell = 5$ curve, it will be assumed here that the $^{90}Zr(d,p)$ data establish the existence of an $h_{11/2}$ state at 2.16 MeV. A summary of the $^{90}Zr(^{16}O,^{15}O)$ results, compared with those from the $^{90}Zr(d,p)$ and $^{90}Zr(\alpha,^3He)$ reactions, is given in Table VII.

The contribution to the 2.16 MeV peak from the unresolved $\nu g_{7/2}$ state at 2.19 MeV cannot be obtained from the data. However, it can be estimated with the help of the $^{92}Mo(^{16}O,^{15}O)^{93}Mo$ data presented below (Sec. III-J). In the $^{92}Mo(^{16}O,^{15}O)$ spectrum the $\nu g_{7/2}$ and $\nu h_{11/2}$ levels are no longer degenerate

but are separated by about 800 keV. The spectroscopic factors for the $g_{7/2}$ levels at 1.359 and 1.516 MeV, 0.26 and 0.14, respectively,[39] are about the same as that for the unresolved $g_{7/2}$ state at 2.19 MeV in ^{91}Zr, whose spectroscopic factor is 0.48.[36] Similarly, the $\ell = 5$ spectroscopic factors for the ^{91}Zr 2.16 MeV state and ^{93}Mo 2.32 MeV state are 0.37 and 0.33, respectively.[36,39] From the cross section ratio of the 1.5 and 2.3 MeV groups in ^{93}Mo, we can then estimate that about 20% of the 2.16 MeV peak in the $^{90}Zr(^{16}O,^{15}O)^{91}Zr$ reaction is due to the $\nu g_{7/2}$ state at 2.19 MeV. This is only a rough estimate but it does justify the assumption that the peak in the $^{90}Zr(^{16}O,^{15}O)$ data at 2.16 MeV is mainly $h_{11/2}$. An explanation for the dominance of the $h_{11/2}$ over the $g_{7/2}$ state can be found in the selection rules, which allow L = 6 for the $h_{11/2}$ state and L = 3 for the $g_{7/2}$. In a situation of poor momentum matching (the favored $(^{16}O,^{15}O)$ L transfer at these Q-values is about 10) the high spin states will be closer to the favored conditions than the lower spin states and thus are preferred.

The higher states seen in the $^{90}Zr(^{16}O,^{15}O)^{91}Zr$ reaction are all quite weak. The 2.7 MeV state seen in the $(^{16}O,^{15}O)$ data with about 3% of the ground state cross section could correspond to the 2.8 MeV, $\ell = 2$ state in the $^{90}Zr(d,p)$ data[35] with a spectroscopic factor about 1/30 that of the ground state. The level in the ^{15}O spectrum at 3.4 MeV probably corresponds to the $g_{7/2}$ state observed at 3.47 MeV in the $^{90}Zr(d,p)$ reaction.[35,36] Similarly, $\ell = 5$ levels have been reported[36] near 4.1 MeV. Above this point the level density is too high to attempt to compare the $^{90}Zr(^{16}O,^{15}O)$ data with the light ion results.

J. $^{92}Mo(^{16}O,^{15}O)^{93}Mo$

The $^{92}Mo(^{16}O,^{15}O)^{93}Mo$ reaction was observed at $\theta_\ell = 20$ and 25°. A spectrum at $\theta_\ell = 20°$ is shown in Fig. 15. The resolution is about 250 keV

(FWHM). Included in Fig. 15 is a spectrum from the $^{92}Mo(\alpha,^{3}He)^{93}Mo$ reaction at 65 MeV. As was true for the $^{90}Zr(^{16}O,^{15}O)^{91}Zr$ data, very few levels are populated strongly. A summary of the levels observed in the $^{92}Mo(^{16}O,^{15}O)$ reaction and their intensities is given in Table VIII.

The $^{92}Mo(d,p)^{93}Mo$ reaction has been studied by Moorhead and Moyer,[39] who assigned the 2.32 MeV level as $\ell = 5$ ($h_{11/2}$). Booth et al.[37] also assigned $\ell = 5$ to this level in the $^{92}Mo(d,p)$ reaction. The complementary $^{94}Mo(d,t)$ reaction has been studied by Diehl et al.[40] in order to confirm the assignments from (d,p) for the low-lying levels in ^{93}Mo. The 0.94 MeV state was found to be the strongest $\ell = 0$ transition, with a spectroscopic factor of 0.64. Near 1.5 MeV several states are reported. From a comparison of the $^{92}Mo(d,p)$ and $^{94}Mo(d,t)$ data the levels are:[39,40] 1.359 MeV($7/2^+$), 1.489 MeV($9/2^+$), 1.502 MeV($3/2^+$), and 1.529 MeV($7/2^+$). Based on the $(^{16}O,^{15}O)$ selection rules, the $9/2^+$ would be the favored transition (L = 5). However, this is a $\nu g_{9/2}^{-1}$ state, since it was populated strongly in the (d,t) experiment and not observed at all in the (d,p) data. Of the remaining states, it seems likely that the $g_{7/2}$ (L = 3) would be stronger than the $d_{3/2}$ (L = 1) in a situation where the momentum matching for low L transfers is poor. From Fig. 15 it is obvious that the relative intensities of the doublet at 1.5 MeV in the $^{92}Mo(^{16}O,^{15}O)$ reaction cannot be explained by populating only the $g_{7/2}$ states. The 1.36 MeV $7/2^+$ state has a larger spectroscopic factor than does the 1.53 MeV $7/2^+$ state,[39] while the $(^{16}O,^{15}O)$ data show more intensity to the upper level by roughly a factor of 2. (This is also true for the $^{92}Mo(\alpha,^{3}He)$ data in Fig. 15.) Whether the intensity of the 1.5 MeV state seen here is due to population of the $d_{3/2}$ state or to the appearance of the 1.49 MeV $g_{9/2}$ state cannot be determined without greatly improved experimental resolution. It

should be remarked here that the estimate of the $\nu g_{7/2}$ contribution to the 2.16 MeV peak in the $^{90}Zr(^{16}O,^{15}O)^{91}Zr$ reaction (Sec. III-I) was based on the assumption that all of the observed intensity at 1.5 MeV in ^{93}Mo was due to the $\nu g_{7/2}$ states. Therefore, the estimate of 20% should be considered as an upper limit to the expected contribution.

K. $^{93}Nb(^{16}O,^{15}O)^{94}Nb$

The $^{93}Nb(^{16}O,^{15}O)^{94}Nb$ reaction was observed at θ_ℓ = 20 and 25°. A spectrum at θ_ℓ = 20° is shown in Fig. 16. The resolution was about 250 keV (FWHM). Only three levels were populated strongly. Based on a calibration curve from the $^{93}Nb(^{16}O,^{15}N)^{94}Mo$ reaction, the excitation energies determined for the three strong levels are -0.05, 1.8, and 2.2 MeV. The peak cross sections for these levels are given in Table IX.

The $^{93}Nb(d,p)^{94}Nb$ reaction has been studied by Moorhead and Moyer[39] and by Sheline et al.[41] The low-lying levels are interpreted as being a multiplet whose main configuration is $[\pi g_{9/2},(\nu d_{5/2})^3_{5/2}]_{2^+\to 7^+}$. These states are analogous to the low-lying multiplet seen in ^{92}Nb.[4,7,29] However, in ^{94}Nb the states are very close together. Five of the six states lie within 113 keV of the ground state in ^{94}Nb, while in ^{92}Nb the six levels span 500 keV of excitation energy. This explains why the peak in Fig. 16 looks narrow compared with the peak seen in the $^{91}Zr(^{16}O,^{15}N)^{92}Nb$ spectrum (Fig. 11). The cross section obtained for this multiplet in ^{94}Nb is only about half that found for the $^{90}Zr(^{16}O,^{15}O)^{91}Zr$ (g.s.) reaction, although the Q-values are the same in the two cases. In the $^{93}Nb(^{16}O,^{15}O)$ reaction, however, the presence of two $d_{5/2}$ neutrons in the target ground state will reduce the $\nu d_{5/2}$ cross section compared with that in the $^{90}Zr(^{16}O,^{15}O)$ reaction, since there are only 4 holes

in the $d_{5/2}$ shell (in a simple picture) rather than 6. Moreover, there is expected[41] to be mixing between the $(\nu d_{5/2})^3_{5/2^+}$, $(\nu d_{5/2})^3_{3/2^+}$, and $(\nu d_{5/2})^3_{9/2^+}$ configurations which will remove some of the $\nu d_{5/2}$ strength from the ground state multiplet. (The ^{93}Nb(d,p) data indicate[42] ℓ = 2 strength up to 1.5 MeV.)

The excitation energy obtained here for the $\nu d_{5/2}$ multiplet is incorrect due to there being no known states to include in the calibration curve. (In most other reactions at least the ground state could be used as a calibration point. While the overlap of known points from various runs was never perfect, it was always possible to obtain reasonable excitation energy values when there were known points from each of the spectra being calibrated.) An estimate of the true excitation energy of the -0.05 MeV peak would be the centroid of the states seen in the ^{93}Nb(d,p) reaction. From Ref. 39 this is about 0.06 MeV. Thus, the excitation energies reported for the three states seen here are estimated to be low by about 110 keV.

The strength of the groups near 2 MeV in the (^{16}O,^{15}O) data argues strongly for a ($\pi g_{9/2}$,$\nu h_{11/2}$) multiplet at this energy in ^{94}Nb. As is clearly evident from the ^{92}Mo(^{16}O,^{15}O) data (Fig. 15) only the $\nu h_{11/2}$ transition is comparable in intensity to the $\nu d_{5/2}$ transition. The energy differences between the $\nu d_{5/2}$ and $\nu h_{11/2}$ groups in the ^{90}Zr(^{16}O,^{15}O) and ^{92}Mo(^{16}O,^{15}O) reactions, 2.2 and 2.3 MeV, respectively, agree quite well with the 2.1 MeV difference between the strong groups in the ^{93}Nb(^{16}O,^{15}O) data. No ℓ = 5 neutron transfers have been reported in the ^{93}Nb(d,p) reaction, but the cross sections for such transitions were estimated[39] to be less than 70 μb/sr at a deuteron energy of 12 MeV.

L. ^{94}Zr(^{16}O,^{15}O)^{95}Zr

The ^{94}Zr(^{16}O,^{15}O)^{95}Zr reaction was observed only at θ_ℓ = 25°. The spectrum, obtained from the ^{15}O(7+) charge state, is shown in Fig. 17, along

with $^{15}O(7+)$ spectra from the ^{90}Zr and ^{91}Zr targets. Because only the 7+ charge state was observed, the amount of data is rather small. Still, it was possible to identify the ground and 2.0 MeV states in ^{95}Zr.

The $^{94}Zr(d,p)^{95}Zr$ reaction was studied by Cohen and Chubinsky.[34] The ground state was found to be a $\nu d_{5/2}$ level with a spectroscopic factor S = 0.30. As would be expected from a simple picture of the Zr isotopes, the spectroscopic factor of the $\nu d_{5/2}$ transition decreases about a factor of 3 in going from ^{90}Zr (6 holes in the $\nu d_{5/2}$ shell) to ^{94}Zr (2 holes in the $\nu d_{5/2}$ shell).

The 2.03 MeV state seen by Cohen and Chubinsky[34] was assigned $\ell = 4$ ($g_{7/2}$). From the "systematics" of the (^{16}O,^{15}O) reaction observed here, strong population of a $\nu g_{7/2}$ state would be unlikely. However, the 2.02 MeV state seen by Booth et al.[37] was assigned $\ell = 5$ ($h_{11/2}$), which agrees with the observed preference (see Secs. III-I and III-J) for the (^{16}O,^{15}O) reaction to populate $\nu h_{11/2}$ states.

As discussed earlier, there are serious difficulties in attempting to obtain cross section information from data corresponding to ions which are not fully stripped (see Sec. II-D). However, in this case no data from the $^{15}O(8+)$ charge state were obtained. In order to obtain at least an estimate of the cross sections for this reaction, the data were corrected with values of $R_{8/7}$ obtained from Sec. II-D, Eq. (4b). Because of the possible error in this procedure, an arbitrary 50% error is given to these corrected values. Both the uncorrected and corrected cross sections are given in Table X.

M. $^{91}Zr(^{16}O,^{15}O)^{92}Zr$

The $^{91}Zr(^{16}O,^{15}O)^{92}Zr$ reaction was observed (with the $^{15}O(7+)$ charge state) only at $\theta_\ell = 25°$. The spectrum is included in Fig. 17. Three states,

at 0.9, 1.5, and 3.5 MeV, were identified. Their intensities, both uncorrected and corrected for charge state, are given in Table XI.

The $^{91}Zr(d,p)^{92}Zr$ reaction[34,36] indicates that the 0.0, 0.936, and 1.495 MeV levels are mainly $(\nu d_{5/2})^2$ states with spins of 0^+, 2^+, and 4^+ respectively. The expected $(2J_f + 1)$ dependence of the stripping cross sections, which is followed rather well for these states in the (d,p) data, is the probable explanation for the lack of an identifiable ground state peak. The $(^{16}O,^{15}O)$ cross sections of the 0.9 and 1.5 MeV peaks also follow the $(2J_f + 1)$ rule almost exactly.

In the region near 3.5 MeV there were several $\ell = 5$ transitions observed by Bingham and Halbert.[36] The strongest of these was at 3.581 MeV. It seems reasonable to associate the 3.5 MeV level seen here with this $h_{11/2}$ state, based on the observed selectivity of the $(^{16}O,^{15}O)$ reaction in strongly populating only $\nu d_{5/2}$ and $\nu h_{11/2}$ states in the other targets studied.

N. $(^{16}O,^{17}O)$ Reactions

Due to the method of gating employed with the heavy ion focal plane detector (see Sec. II-C), there can arise certain ambiguities in the particle identification. An example of this is $^{17}O(8+)$ and $^{15}O(7+)$, which have the same Z and (within the 5 ns TOF resolution of the detector) the same value for M/q. If the Q-values for the $(^{16}O,^{15}O)$ and $(^{16}O,^{17}O)$ reactions are appropriate, they will fall in different regions of the focal plane and can therefore be observed simultaneously. Such is the case for the $(^{16}O,^{17}O)$ reaction on most of the Zr isotopes. Peaks corresponding to the $(^{16}O,^{17}O)$ reaction (leading to the ground state of the final nucleus) have been observed for ^{91}Zr, ^{92}Zr, ^{94}Zr, and possibly ^{96}Zr. These peaks were all observed in the $^{15}O(7+)$ gate set for the ^{90}Zr

target at $\theta_\ell = 25°$. They are labeled in Fig. 17. (The small peak between the ^{90}Zr and ^{93}Zr ground state peaks has a position appropriate for the $^{96}Zr(^{16}O,^{17}O)^{95}Zr$ ground state, although it corresponds to a very large cross section. Compared with the other $(^{16}O,^{17}O)$ cross sections determined here, however, it does not appear to be unreasonably large.)

Fortunately, it was possible to confirm the identity of some of the ^{17}O peaks seen in Fig. 17 by observing them in the $^{15}O(7+)$ gates of the other targets studied. Based on the isotopic abundances from Ref. 4, cross sections for all of the ^{17}O peaks were calculated for the ^{90}Zr target. In the case of the $^{91}Zr(^{16}O,^{17}O)$ and $^{94}Zr(^{16}O,^{17}O)$ reactions (also in Fig. 17), the cross sections calculated from the ^{90}Zr target agreed quite well with those from the ^{91}Zr and ^{94}Zr targets. No confirmation for the $^{92}Zr(^{16}O,^{17}O)$ or $^{96}Zr(^{16}O,^{17}O)$ cross section was possible since these targets were not used in the heavy ion experiments. The cross sections obtained for the $(^{16}O,^{17}O)$ reaction on the various targets are summarized in Table XII.

In the $^{91}Zr(^{16}O,^{17}O)$ reaction (Fig. 17), a peak corresponding to the ^{17}O first excited state at 0.87 MeV was also observed. For all of the other cases, the Q-value was such that the ^{17}O 0.87 MeV peak was off the detector. Although the ^{17}O excited state was only observed once, its interpretation seems unambiguous. The intensity of the peak is roughly a factor of 20 higher than can be accounted for by an isotopic impurity, and the excitation energy, 0.9 MeV, cannot correspond to a state in the residual nucleus since the first excited state of ^{90}Zr is at 1.75 MeV. (Furthermore, the cross section for the 1.75 MeV 0^+ state in the $^{91}Zr(p,d)$ reaction[43] was less than 10^{-3} that of the ground state.) The cross section observed for the $^{91}Zr(^{16}O,^{17}O^*)^{90}Zr(g.s.)$ reaction was 22% of that for the $^{91}Zr(^{16}O,^{17}O)^{90}Zr(g.s.)$ reaction. From the

selection rules, the latter reaction ($d_{5/2} \rightarrow d_{5/2}$ transition) can have contributions from L = 0, 2, and 4, while the former reaction ($d_{5/2} \rightarrow s_{1/2}$ transition) is restricted to L = 2. The factor of 5 difference in cross section between the two reactions may be related to the preference for high L transfers ($\sigma_{L+2} \approx 10\ \sigma_L$) suggested by DWBA calculations.[9]

The trend in ($^{16}O,^{17}O$) cross sections with mass number can be qualitatively understood in terms of the filling of the $\nu d_{5/2}$ shell. In a simple picture the cross sections should be in the ratio 1:2:4:6 in going from ^{91}Zr to ^{96}Zr. With the exception of the ^{91}Zr to ^{92}Zr ratio, the experimental results (Table XII) are in reasonable agreement with this prediction.

The states observed here were also seen in the ($^{16}O,^{17}O$) data of Christensen et al.[27] at 60 MeV. They report peak cross sections of 0.77, 2.13, and 8.4 mb/sr for the ^{92}Zr, ^{94}Zr, and ^{96}Zr targets, respectively. Since the $^{94}Zr(^{16}O,^{17}O)^{93}Zr$(g.s.) cross section seen here is a factor of 10 larger than that reported at 60 MeV, a > 50 mb/sr cross section for the $^{96}Zr(^{16}O,^{17}O)^{95}Zr$(g.s.) transition appears reasonable compared with the 8 mb/sr cross section observed in the lower energy experiment.

IV. CORE EXCITATION

The 60 MeV ($^{16}O,^{15}N$) data obtained by Nickles et al.[2] on the Zr isotopes were compared with the (^{3}He,d) data of Cates, Ball, and Newman[7] in order to find the single-particle states in the odd Nb isotopes. The (α,t) data (Refs. 3 and 4) on the same targets, however, showed many strong levels which were not reported in the (^{3}He,d) reaction. The reason for the difference in the (^{3}He,d) and (α,t) results is related to the different momentum matching in the two reactions, the (^{3}He,d) reaction preferentially populating low angular momentum ($\ell \leq 2$) states and the (α,t) reaction preferentially populating high

angular momentum ($\ell \geq 3$) states. As was mentioned earlier, the favored momentum transfer for the (^{16}O,^{15}N) reaction, $L \approx 3$, suggests that the (^{16}O,^{15}N) data should be compared with (α,t) as well as (^{3}He,d) data, in order to better reproduce the "momentum matching" features of the heavy ion reaction. Table XIII lists the core-excited levels suggested by Nickles et al.[2] along with nearby strong states seen in the (α,t) reaction. As can be seen, essentially all of the levels reported in the (^{16}O,^{15}N) reaction also appear as strong (α,t) transitions. The levels at 2.18 and 2.75 MeV in $^{90}Zr(^{16}O,^{15}N)^{91}Nb$ may not have counterparts in the (α,t) data. However, neither of these states was observed in the present $^{90}Zr(^{16}O,^{15}N)$ experiment (see Fig. 6).

It is clear from the heavy ion data obtained in the experiments reported here that the preference for high angular momentum transfer is less pronounced than for the (α,t) reaction. As an example, consider the $^{90}Zr(^{16}O,^{15}N)^{91}Nb$ results. The intensity of the 3.37 MeV ($2d_{5/2}$) state is greater relative to that of the ground state ($1g_{9/2}$) than was true for the $^{90}Zr(\alpha,t)$ reaction. Moreover, the cross section for the 3.37 MeV ($2d_{5/2}$) state (L = 3) is much larger compared with that of the 4.81 MeV ($1g_{7/2}$) state (L = 3) in the heavy ion than in the light ion data. An explanation for these observations is that heavy ion reactions, because they occur in a region well outside the nucleus, are more sensitive to the "tail" of the nuclear wave function than are light ion reactions. The magnitude of the nuclear wave function at a given radius, however, depends on both the quantum numbers n and ℓ. For a given radial quantum number, n, the wave function peaks at a larger radius as ℓ increases. On the other hand, increasing the number of radial nodes of a wave function (i.e., increasing n) will also cause it to have a larger amplitude at large radius. Based on data from the $^{208}Pb(^{16}O,^{15}N)$ reaction,[9] it appears

that the effect of an extra radial node is approximately the same as the effect of two additional units of transferred angular momentum.

In the case of the $^{90}Zr(^{16}O,^{15}N)^{91}Nb$ reaction, if we divide the observed cross sections for the ground and 3.37 MeV states by the values of $(2J_f + 1)C^2S$ from Ref. 44, we obtain reduced cross sections of $\sigma_R(1g_{9/2}) = 0.5$ and $\sigma_R(2d_{5/2}) = 0.7$. The same calculation using the $^{90}Zr(\alpha,t)$ cross sections yields $\sigma_R(1g_{9/2}) = 0.4$ and $\sigma_R(2d_{5/2}) = 0.1$. Thus, in (α,t) we would expect that the $1g_{9/2}$ cross section would be about 4 times larger than that for a $2d_{5/2}$ state with the same spectroscopic factor, while in $(^{16}O,^{15}N)$ the states would be populated about equally. This argument is not meant to be quantitative, since Q-value effects have been ignored. However, for similar Q-values the estimates above are probably reasonable. From the $(^{16}O,^{15}N)$ selection rules (Eq.(12)), a $1g_{7/2}$ and $2d_{5/2}$ state require the same L transfer, and in this case the $2d_{5/2}$ state (with the extra radial node) is favored. A nice example of this effect can be found in the $^{92}Mo(^{16}O,^{15}O)^{93}Mo$ spectrum (Fig. 15). (The $(^{16}O,^{15}O)$ and $(^{16}O,^{15}N)$ reactions have identical selection rules.) The ground state of ^{93}Mo is $2d_{5/2}$, the states near 1.5 MeV are $1g_{7/2}$, and the 2.32 MeV state is $1h_{11/2}$. Comparison with the $^{92}Mo(\alpha,^3He)$ spectrum (also in Fig. 15) shows that, relative to the $1h_{11/2}$ level, the $2d_{5/2}$ state is stronger in the heavy ion data, while the $1g_{7/2}$ states are considerably weaker compared with both the $2d_{5/2}$ and $1h_{11/2}$ levels.

The $^{94}Zr(^{16}O,^{15}N)^{95}Nb$ data obtained here show population of the same states observed by Nickles et al.[2] In $^{94}Zr(\alpha,t)$, the 0.74 - 0.82 MeV ($\ell = 1$) doublet had about twice the intensity of the 0.25 MeV ($\ell = 1$) state. Based on the results of fitting the ground state peak as a doublet, this ratio is essentially the same in the $^{94}Zr(^{16}O,^{15}N)$ data (see Table IV). Similarly, the 1.65 and 2.10 MeV states, which were strong in the (α,t) reaction,[4] are also strong

in the (^{16}O,^{15}N) reaction. The 1.27 MeV level in ^{94}Zr(α,t), which had about 8% of the ground state intensity, looks weaker in the heavy ion data (assuming it corresponds to the 1.1 MeV level). However, the intensity ratio of the 1.1 MeV state to the ground state, about 5%, does not differ greatly from the light ion ratio. The 2.0 MeV state appears relatively stronger in the heavy ion data, but this would occur even for $d_{5/2}$ states, for example, which would be expected to begin to appear at about this excitation energy. A strong $d_{5/2}$ state, of course, should have been observed in ^{94}Zr(^{3}He,d), but only levels up to 1.26 MeV were reported in Ref. 7.

The apparent absence of the 0.68 MeV level in the ^{92}Mo(^{16}O,^{15}N) data provides an argument against the importance of a multi-step reaction mechanism for this reaction. This state may correspond to the $(\pi g_{9/2})^3$ $7/2^+$ state calculated[45-47] to lie at about 0.7 MeV in ^{93}Tc. Consistent with this hypothesis is the extremely weak population of the 0.68 MeV state in ^{92}Mo(^{3}He,d)[48,49] and its relatively stronger population in ^{92}Mo(α,t).[3] If this $7/2^+$ state is populated through a $\pi g_{7/2}$ admixture, its weakness (compared with the $1g_{9/2}$ and $2d_{5/2}$ states) in the (^{16}O,^{15}N) reaction would be expected, based on the arguments given above. On the other hand, if a multistep mechanism were important, the transition could proceed by a $\pi g_{9/2}$ transfer along with uncoupling the $(g_{9/2})^2_{0^+}$ protons. Figure 9 indicates that the likelihood of such a process is small. Particularly in ^{93}Nb, there is experimental evidence[50] that the low-lying states do have appreciable admixtures of the core-excited configuration [^{92}Zr(2+) ⊗ $\pi g_{9/2}$], but the (α,t) levels at 0.80 MeV ($5/2^+$) and 0.95 MeV ($9/2^+$) could account for the (^{16}O,^{15}N) state reported by Nickles et al.[2] at 0.93 MeV.

An estimate of the importance of a multi-step reaction mechanism can

also be made in the case of the $^{90}Zr(^{16}O,^{15}O)^{91}Zr$ reaction. From Fig. 13 it is obvious that only two levels are strongly populated, the same two levels which are strongly populated in the $^{90}Zr(\alpha,^{3}He)$ reaction. The locations of core-excited levels in ^{91}Zr have been determined by DuBard and Sheline[38] with the $^{91}Zr(p,p')$ reaction. They find that the 2.16 MeV level is indeed a member of the $[^{90}Zr(3^-) \otimes \nu d_{5/2}]$ multiplet, as are the states at 2.630 MeV ($1/2^-$), 2.683 MeV ($7/2^-$), 2.800 MeV ($9/2^-$), 2.821 MeV ($5/2^-$), and 3.022 MeV ($3/2^-$). As is evident from Fig. 13, only one member of this core-excited multiplet is populated with reasonable intensity. It seems unlikely that only the $11/2^-$ state (which is known[36,37] to have an appreciable $\nu h_{11/2}$ single-particle amplitude) would be strongly populated in the $(^{16}O,^{15}O)$ reaction if core-excitation were an important part of the reaction mechanism. The $^{92}Mo(^{16}O,^{15}O)$ reaction (Fig. 15) also yields a spectrum very similar to that from the $(\alpha,^{3}He)$ reaction. Although it has not been experimentally verified, it is quite likely that the 2.32 MeV $11/2^-$ state in ^{93}Mo is also partly a $[^{92}Mo(3^-) \otimes \nu d_{5/2}]$ level. Here too, no other levels except the known single-particle states are observed.

From the comparisons made above it must be concluded that, contrary to the suggestion of Nickles et al.,[2,27] there is no strong evidence for the population of states which do not have single-particle strength.

V. DWBA ANALYSIS

A. Expression for Cross Section

Under certain assumptions the cross section for nucleon transfer between heavy ions

$$\underset{(a_1)}{(c_1 + t)} + c_2 \rightarrow \underset{(a_2)}{(c_2 + t)} + c_1 \qquad (14)$$

can be written as[21,22,51]

$$\frac{d\sigma}{d\Omega} = \frac{(2a_2 + 1)(2j_1 + 1)}{(2c_2 + 1)(2j_2 + 1)} \mathcal{S}_1 \mathcal{S}_2 \sum_L (2L + 1) \frac{(j_1 \tfrac{1}{2} L0 | j_2 \tfrac{1}{2})^2}{(2j_2 + 1)} \sigma_L(\theta) \tag{15}$$

where L is the transferred angular momentum, c_2, a_2 are the spins of the target and residual nuclei, and $\mathcal{S}_1 \ell_1 j_1$, $\mathcal{S}_2 \ell_2 j_2$ are the spectroscopic factor, orbital, and total angular momenta of the transferred nucleon in the projectile and final nucleus, respectively. The quantity $\sigma_L(\theta)$ is the DWBA cross section for the transition $\ell_1 j_1 \rightarrow \ell_2 j_2$ proceeding by the angular momentum transfer L, as calculated by the program DWUCK.[52] The expression for the cross section given in Eq. (15) neglects recoil terms, which are of the order M_t/M_{a_1}, and results in the selection rules given in Sec. III-A, Eqs. (9)-(11). The calculations reported here use the finite-range form factor described in Ref. 22. The present experiments were performed at incident energies well above the Coulomb barrier involving a variety of projectiles and therefore provide a good test of the no-recoil DWBA theory.

B. Proton Transfers

The results of calculations for the $^{90}Zr(^{16}O,^{15}N)^{91}Nb$ reaction are shown in Fig. 7. The spectroscopic factors deduced for ^{91}Nb levels are given in Table XIV ($\mathcal{S}_2 \equiv C^2S^2$) where we have normalized the DWBA calculations to $\mathcal{S}_2 = 1$ for the ^{91}Nb g.s. transition. The optical model parameters were taken from Ref. 27. These parameters were found to fit the measured elastic scattering. The bound state parameters are also listed in Table XIV. As can be seen from Fig. 7, the DWBA calculations fit quite well. Unfortunately, there are no reliable L-signatures. Therefore in the DWBA calculations we have calculated spectroscopic factors assuming different values for $n_2 \ell_2 j_2$ which are consistent with

ℓ_2 values deduced from light ion reactions. Also listed in Table XIV are the results obtained for (^{12}C,^{11}B), again normalized to the ^{91}Nb ground state, and results from the ^{90}Zr(^3He,d) reaction.[7,44]

The values of $\mathcal{S}_2$ deduced for ^{91}Nb states with $j_2 = \ell_2 + 1/2$ are in satisfactory agreement with those from (^3He,d) for both (^{16}O,^{15}N) and (^{12}C,^{11}B). However, the spectroscopic factors deduced from the (^{16}O,^{15}N) data for known states with $j_2 = \ell_2 - 1/2$, e.g., the 1.84 MeV $f_{5/2}$ state and the 4.80 MeV $g_{7/2}$ state, are too large by about a factor of 25. The j-values for the ^{91}Nb levels at 4.2 and 5.3 MeV are not well-established from (^3He,d). If we exclude the (^{16}O,^{15}N) calculations for $j_2 = \ell_2 - 1/2$, our results are most consistent with these states having $j_2 = \ell_2 - 1/2$ since they are populated strongly (relative to the 3.37 MeV $d_{5/2}$ state) in (^{12}C,^{11}B).

Table XV lists the results of a DWBA analysis of the ^{92}Mo(^{16}O,^{15}N) and ^{92}Mo(^{12}C,^{11}B) reactions, compared with spectroscopic factors obtained from (^3He,d).[49] The parameters and normalizations are the same as those employed in Table XIV. Again there is satisfactory agreement for levels with $j_2 = \ell_2 + 1/2$ whereas $\mathcal{S}_2$ for the $p_{1/2}$ level is greatly overestimated in (^{16}O,^{15}N) and underestimated in (^{12}C,^{11}B). The results for the 3.8 MeV level appear to favor a $d_{3/2}$ or $g_{7/2}$ assignment, as do those for the 4.8 MeV level. A $g_{7/2}$ (or $g_{9/2}$) assignment to the 3.8 and 4.8 MeV states would be consistent with their being the high-spin levels seen in ^{92}Mo(α,t) near these energies.[3]

C. Neutron Transfers

Calculations for the $^{90}Zr(^{16}O,^{15}O)^{91}Zr$ reaction are shown in Fig. 14. Spectroscopic factors ($\mathcal{S}_2 \equiv C^2S_2$) obtained for ($^{16}O,^{15}O$) are included in Tables VII, VIII, and X along with (d,p) results. The same systematic features as noted for ($^{16}O,^{15}N$) are observed, in particular the spectroscopic factors for states with $j_2 = \ell_2 - 1/2$ are greatly overestimated.

The discrepancy in spectroscopic factors between states with $j_2 = \ell_2 + 1/2$ and $j_2 = \ell_2 - 1/2$ deduced from ^{16}O stripping reactions has been observed in other mass regions.[9,27] It appears to be a consequence of the no-recoil selection rules (Sec. III-A, Eqs. (9)-(11)) which restrict the allowed L transfers. The effect is greatest for ($^{16}O,^{15}N$) or ($^{16}O,^{15}O$) reactions ($p_{1/2}$ transfer) leading to states with $j_2 = \ell_2 - 1/2$ since the L transfer allowed by the selection rules is generally smaller than the kinematically favored value. For the ^{16}O stripping reactions to states with $j_2 = \ell_2 + 1/2$ and the ($^{12}C,^{11}B$) reaction ($p_{3/2}$ transfer) where larger L-values are allowed by the no-recoil selection rules, the calculated cross sections are not so strongly affected by ignoring the recoil terms. Inclusion of recoil effects[53-55] allows L transfers normally restricted by the parity selection rule, Sec. III-A, Eq. (11). For the ($^{16}O,^{15}N$) and ($^{12}C,^{11}B$) reactions, then, $L = \ell_2$ is allowed. Since usually $\sigma_{L+1} >> \sigma_L$, the recoil term is most important for reactions where the no-recoil selection rules require $L < \ell_2$, which is consistent with the present observations. A DWBA analysis including recoil effects as suggested in Ref. 54 will be presented at a later date. It appears, however, that no-recoil DWBA calculations may be useful for reactions leading to states where the no-recoil selection rules allow $L > \ell_2$, e.g., ($^{12}C,^{11}B$) reactions or ($^{16}O,^{15}N$) reactions to states with $j_2 = \ell_2 + 1/2$.

D. Transfers to Projectile Excited States

In the (^{16}O,^{15}N) and (^{12}C,^{11}B) reactions groups were observed which are most likely due to transfers to excited states in ^{15}N and ^{11}B, respectively. It is thus possible to obtain spectroscopic information about these states using Eq. (15). In Table XVI we list values for $\mathcal{S}_1$ deduced for the ^{15}N $p_{3/2}^{-1}$ state at 6.33 MeV and the ^{11}B $p_{1/2}$ state at 2.12 MeV, assuming that these are the (Doppler broadened) levels seen in Figs. 6 and 9. The results are in fair agreement with other measurements. In both cases $L > \ell_2$ is allowed so that recoil effects should be minimal.

E. Comparison between Different Reactions

Since we are using finite-range DWBA it is possible to deduce projectile ground state spectroscopic factors by comparing the DWBA normalization factors obtained for the different reactions. Although the absolute normalization of the DWBA cross sections was not attempted, we have compared spectroscopic factors for ^{15}O (g.s.) and ^{11}B (g.s.) relative to ^{15}N (g.s.). These are also listed in Table XVI. The relative values of $\mathcal{S}_1$ listed depend somewhat on the bound state parameters used.[31] This effect has interesting possibilities; the comparison of (^{16}O,^{15}N) and (^{16}O,^{15}O) could yield accurate information about the proton and neutron single-particle potentials in nuclei since the projectiles are mirror nuclei.

The results given in Table XVI indicate that it is feasible to deduce spectroscopic information from different heavy ion reactions by using finite-range DWBA with a common normalization. This is in contrast to light-ion reactions where it is found necessary to use separate DWBA normalization factors for each reaction studied.[52] The DWBA normalization used here for (^{16}O,^{15}N)

C. Neutron Transfers

Calculations for the $^{90}Zr(^{16}O,^{15}O)^{91}Zr$ reaction are shown in Fig. 14. Spectroscopic factors ($\mathcal{S}_2 \equiv C^2S_2$) obtained for ($^{16}O,^{15}O$) are included in Tables VII, VIII, and X along with (d,p) results. The same systematic features as noted for ($^{16}O,^{15}N$) are observed, in particular the spectroscopic factors for states with $j_2 = \ell_2 - 1/2$ are greatly overestimated.

The discrepancy in spectroscopic factors between states with $j_2 = \ell_2 + 1/2$ and $j_2 = \ell_2 - 1/2$ deduced from ^{16}O stripping reactions has been observed in other mass regions.[9,27] It appears to be a consequence of the no-recoil selection rules (Sec. III-A, Eqs. (9)-(11)) which restrict the allowed L transfers. The effect is greatest for ($^{16}O,^{15}N$) or ($^{16}O,^{15}O$) reactions ($p_{1/2}$ transfer) leading to states with $j_2 = \ell_2 - 1/2$ since the L transfer allowed by the selection rules is generally smaller than the kinematically favored value. For the ^{16}O stripping reactions to states with $j_2 = \ell_2 + 1/2$ and the ($^{12}C,^{11}B$) reaction ($p_{3/2}$ transfer) where larger L-values are allowed by the no-recoil selection rules, the calculated cross sections are not so strongly affected by ignoring the recoil terms. Inclusion of recoil effects[53-55] allows L transfers normally restricted by the parity selection rule, Sec. III-A, Eq. (11). For the ($^{16}O,^{15}N$) and ($^{12}C,^{11}B$) reactions, then, $L = \ell_2$ is allowed. Since usually $\sigma_{L+1} >> \sigma_L$, the recoil term is most important for reactions where the no-recoil selection rules require $L < \ell_2$, which is consistent with the present observations. A DWBA analysis including recoil effects as suggested in Ref. 54 will be presented at a later date. It appears, however, that no-recoil DWBA calculations may be useful for reactions leading to states where the no-recoil selection rules allow $L > \ell_2$, e.g., ($^{12}C,^{11}B$) reactions or ($^{16}O,^{15}N$) reactions to states with $j_2 = \ell_2 + 1/2$.

D. Transfers to Projectile Excited States

In the (^{16}O,^{15}N) and (^{12}C,^{11}B) reactions groups were observed which are most likely due to transfers to excited states in ^{15}N and ^{11}B, respectively. It is thus possible to obtain spectroscopic information about these states using Eq. (15). In Table XVI we list values for $\mathcal{S}_1$ deduced for the ^{15}N $p_{3/2}^{-1}$ state at 6.33 MeV and the ^{11}B $p_{1/2}$ state at 2.12 MeV, assuming that these are the (Doppler broadened) levels seen in Figs. 6 and 9. The results are in fair agreement with other measurements. In both cases $L > \ell_2$ is allowed so that recoil effects should be minimal.

E. Comparison between Different Reactions

Since we are using finite-range DWBA it is possible to deduce projectile ground state spectroscopic factors by comparing the DWBA normalization factors obtained for the different reactions. Although the absolute normalization of the DWBA cross sections was not attempted, we have compared spectroscopic factors for ^{15}O (g.s.) and ^{11}B (g.s.) relative to ^{15}N (g.s.). These are also listed in Table XVI. The relative values of $\mathcal{S}_1$ listed depend somewhat on the bound state parameters used.[31] This effect has interesting possibilities; the comparison of (^{16}O,^{15}N) and (^{16}O,^{15}O) could yield accurate information about the proton and neutron single-particle potentials in nuclei since the projectiles are mirror nuclei.

The results given in Table XVI indicate that it is feasible to deduce spectroscopic information from different heavy ion reactions by using finite-range DWBA with a common normalization. This is in contrast to light-ion reactions where it is found necessary to use separate DWBA normalization factors for each reaction studied.[52] The DWBA normalization used here for (^{16}O,^{15}N)

has been compared with those used in the analyses of (^{16}O,^{15}N) on ^{208}Pb at 69 and 104 MeV[9] and (^{16}O,^{15}N) on fp-shell nuclei at 60 MeV.[27] The different normalizations are in very good agreement (±20%) and indicate that DWBA theory can account for most of the kinematic effects observed in heavy ion reactions.

VI. CONCLUSIONS

The present Zr(^{16}O,^{15}N) results, when compared with the 60 MeV results of Nickles et al.,[2] generally show population of the same states. The cross sections measured at 104 MeV, however, are much larger than those reported at 60 MeV. The (^{16}O,^{15}N) reaction shows a preference for high angular momentum transfers similar to (but not as pronounced as) that shown by the (α,t) reaction. There is also a preference for populating levels with high radial quantum numbers.

The (^{16}O,^{15}O) reaction was also observed on the targets studied here. Although the Q-values for this reaction are very negative, measurable cross sections (1-3 mb/sr) were observed. The data from the ^{90}Zr(^{16}O,^{15}O) and ^{92}Mo(^{16}O,^{15}O) reactions are very similar to those from the (α,^{3}He) reaction on the same targets. The (^{16}O,^{15}O) reaction, at least in this mass region, appears to be an excellent way of observing $\nu h_{11/2}$ levels. The $\nu h_{11/2}$ levels are about 5 to 10 times stronger than $\nu g_{7/2}$ levels in the (^{16}O,^{15}O) reaction, while in the (α,^{3}He) reaction the $\nu h_{11/2}$ and $\nu g_{7/2}$ transitions have comparable intensities.

The (^{16}O,^{17}O) reaction on ^{91}Zr and ^{94}Zr (and possibly on ^{92}Zr and ^{96}Zr, which are present as isotopic impurities in the targets used here) has also been observed. Only the ground state transition was seen in all cases. Outgoing $^{17}O^{*}$ (0.87 MeV) particles were identified in the ^{91}Zr(^{16}O,^{17}O) data, with an intensity about 22% that of the ^{17}O ground state. The cross sections for this

reaction are quite large, more than 20 mb/sr in the case of $^{94}Zr(^{16}O,^{17}O)$. Evidence for the existence of excited outgoing particles was also obtained in the $(^{16}O,^{15}N)$, $(^{16}O,^{16}O')$, and $(^{12}C,^{11}B)$ reactions. In these cases the peaks were very broad, as would be expected for particles which γ decay in flight. However, there was no indication of excited outgoing particles in the $(^{16}O,^{15}O)$ data.

Notably absent in the present data are the proposed core-excited states in ^{91}Nb at 2.18 and 2.75 MeV reported by Nickles et al.[2] Similarly, the 0.68 MeV $(g_{9/2})^3_{7/2^+}$ state in ^{93}Tc was unobserved in the $^{92}Mo(^{16}O,^{15}N)$ data. In the $(^{16}O,^{15}O)$ data on ^{90}Zr and ^{92}Mo, only the $11/2^-$ member of the core-excited multiplet was populated. These $11/2^-$ states have been seen in both (d,p) and $(\alpha,^3He)$ and have significant $\nu h_{11/2}$ single-particle strength.[36,39] Insofar as the other possible core-excited states seen by Nickles et al.[2] all appear as strong (α,t) transitions, it is concluded here that there is no strong evidence for the multi-step mechanism implied by the 60 MeV results.

Finite-range DWBA calculations using the no-recoil approximation indicate that satisfactory results can be obtained for transitions where $L > \ell_2$ is allowed by the no-recoil selection rules. However, spectroscopic factors for transitions which require $L < \ell_2$, e.g., $(^{16}O,^{15}N)$ or $(^{16}O,^{15}O)$ to states where $j_2 = \ell_2 - 1/2$, are greatly overestimated. Calculations with a common normalization reproduce (to within a factor of about 3) the relative cross sections for a variety of reactions: $(^{16}O,^{15}N)$,$(^{16}O,^{15}N^*)$,$(^{16}O,^{15}O)$,$(^{12}C,^{11}B)$ and $(^{12}C,^{11}B^*)$. These results indicate that, with some notable exceptions, DWBA theory is useful for the analysis of heavy ion reactions well above the Coulomb barrier.

ACKNOWLEDGMENTS

We thank F.G. Pühlhofer and J.R. Meriwether for their assistance, C. Maples for the use of the data analysis programs LION and DERTAG, and C. Ellsworth for preparing the targets. We also thank D. Clark, J. Bowen, and the cyclotron crew for providing the heavy ion beams.

REFERENCES

* Work supported by U.S. Atomic Energy Commission.

Present address: Nuclear Physics Laboratory, University of Washington, Seattle, WA 98195.

1. Nuclear Reactions Induced by Heavy Ions, edited by R. Bock and W.R. Hering (North-Holland, Amsterdam, 1970).

2. R.J. Nickles, V.I. Manko, P.R. Christensen, and F.D. Becchetti, Phys. Rev. Letters 26, 1267 (1971).

3. M.S. Zisman and B.G. Harvey, Phys. Rev. C 4, 1809 (1971).

4. M.S. Zisman and B.G. Harvey, Phys. Rev. C 5, 1031 (1972).

5. W. von Oertzen in Nuclear Reactions and Spectroscopy, edited by J. Cerny (Academic Press, New York), to be published.

6. M.S. Zisman, Lawrence Berkeley Laboratory Report No. LBL-1247 (Ph.D. Thesis), 1972 (unpublished).

7. M.R. Cates, J.B. Ball, and E. Newman, Phys. Rev. 187, 1682 (1969).

8. H.J. Körner, G.C. Morrison, L.R. Greenwood, and R.H. Siemssen, Phys. Rev. C 7, 107 (1973).

9. D.G. Kovar, F.D. Becchetti, B.G. Harvey, F.G. Pühlhofer, J. Mahoney, D.W. Miller, and M.S. Zisman, Phys. Rev. Letters 29, 1023 (1972).

10. F.D. Becchetti, N. Baron, P.R. Christensen, V.I. Manko, and R.J. Nickles, in Proc. of the International Conference on Heavy Ion Physics, Dubna, 1971, p. 361.

11. D.L. Hendrie, J.R. Meriwether, F.B. Selph, D.W. Morris, W.S. Flood, and B.G. Harvey, Lawrence Berkeley Laboratory Report No. UCRL-20426 (1970 Annual Report), p. 280.

12. R.E. Hintz, F.B. Selph, W.S. Flood, B.G. Harvey, F.G. Resmini, and E.A. McClatchie, Nucl. Instr. Methods 72, 61 (1969).

13. C.J. Borkowski and M.K. Kopp, Rev. Sci. Instr. 39, 1515 (1968); C.J. Borkowski and M.K. Kopp, IEEE Trans. on Nucl. Sci. NS17, 340 (1970).

14. Available from the General Electric Company (Valley Forge, PA).

15. B.G. Harvey, J. Mahoney, F.G. Pühlhofer, F.S. Goulding, D.A. Landis, J.C. Faivre, D.G. Kovar, M.S. Zisman, J.R. Meriwether, S.W. Cosper, and D.L. Hendrie, Nucl. Instr. Methods 104, 21 (1972).

16. M.P. Baker, J.R. Calarco, N.S. Chant, J.G. Cramer, and S. Hendrickson, University of Washington Nuclear Physics Laboratory Annual Report (1971), p. 49 (unpublished).

17. J.L.C. Ford, Jr., P.H. Stelson, and R.L. Robinson, Nucl. Instr. Methods 98, 199 (1972).

18. F. Pühlhofer, H.L. Harney, and R. Weisenmiller, private communication.

19. L.C. Northcliffe, Ann. Rev. Nucl. Sci. 13, 67 (1963).

20. Least-squares polynomial fitting routine written by C. Maples, Lawrence Berkeley Laboratory (unpublished).

21. P.J.A. Buttle and L.J.B. Goldfarb, Nucl. Phys. 78, 409 (1966).

22. F. Schmittroth, W. Tobocman, and A.A. Golestaneh, Phys. Rev. C 1, 377 (1970).

23. D.G. Kovar, B.G. Harvey, F.D. Becchetti, F. Pühlhofer, J. Mahoney, M.S. Zisman, and M.A. Nagarajan, Bull. Am. Phys. Soc. 17, 902 (1972); D.G. Kovar, private communication.

24. G.C. Morrison, H.J. Körner, L.R. Greenwood, and R.H. Siemssen, Phys. Rev. Letters 28, 1662 (1972).

25. D.K. Scott, P.N. Hudson, P.S. Fisher, C.U. Cardinal, N. Anyas-Weiss, A.D. Panagiotou, P.J. Ellis, and B. Buck, Phys. Rev. Letters 28, 1659 (1972).

26. H. Doubre, D. Royer, M. Arditi, L. Bimbot, N. Frascaria, J.P. Garron, and M. Riou, Phys. Letters 29B, 355 (1969).

27. P.R. Christensen, V.I. Manko, F.D. Becchetti, and R.J. Nickles, submitted to Nucl. Phys.; F.D. Becchetti, P.R. Christensen, V.I. Manko, and R.J. Nickles, Phys. Letters 43B, 279 (1973).

28. Gaussian peak fitting program written by C. Maples, Lawrence Berkeley Laboratory (unpublished).

29. T.S. Bhatia, W.W. Daehnick, and T.R. Canada, Phys. Rev. C 3, 1361 (1971).

30. C.M. Lederer, J.M. Jaklevic, and J.M. Hollander, Nucl. Phys. A169, 449 (1971).

31. P.J.A. Buttle and L.J.B. Goldfarb, Nucl. Phys. A176, 299 (1971).

32. W. von Oertzen, J. de Physique 32, C6-233 (1971).

33. V.I. Manko, F.D. Becchetti, P.R. Christensen, and R.J. Nickles, J. de Physique 32, C6-225 (1971).

34. B.L. Cohen and O.V. Chubinsky, Phys. Rev. 131, 2184 (1963).

35. A. Graue, L.H. Herland, K.J. Lervik, J.T. Nesse, and B.R. Cosman, Nucl. Phys. A187, 141 (1972)

36. C.R. Bingham and M.L. Halbert, Phys. Rev. C 2, 2297 (1970).

37. W. Booth, S.M. Dalgliesh, K.C. McLean, R.N. Glover, and F.R. Hudson, Phys. Letters 30B, 335 (1969).

38. J.L. DuBard and R.K. Sheline, Phys. Rev. 182, 1320 (1969).

39. J.B. Moorhead and R.A. Moyer, Phys. Rev. 184, 1205 (1969).

40. R.C. Diehl, B.L. Cohen, R.A. Moyer, and H.L. Goldman, Phys. Rev. C 1, 2132 (1970).

41. R.K. Sheline, R.T. Jernigan, J.B. Ball, K.H. Bhatt, Y.E. Kim, and J. Vervier, Nucl. Phys. 61, 342 (1965).

42. E.T. Jurney, H.T. Motz, R.K. Sheline, E.B. Shera, and J. Vervier, Nucl. Phys. A111, 105 (1968).

43. J.B. Ball and C.B. Fulmer, Phys. Rev. 172, 1199 (1968).

44. G. Vourvopoulos, R. Shoup, J.C. Fox, and J.B. Ball, in Nuclear Isospin, edited by J.D. Anderson, S.D. Bloom, J. Cerny, and W.W. True (Academic Press, New York, 1969), p. 205.

45. K.H. Bhatt and J.B. Ball, Nucl. Phys. 63, 286 (1965).

46. N. Auerbach and I. Talmi, Nucl. Phys. 64, 458 (1965).

47. J. Vervier, Nucl. Phys. 75, 17 (1966).

48. J. Picard and G. Bassani, Nucl. Phys. A131, 636 (1969).

49. R.L. Kozub and D.H. Youngblood, Phys. Rev. C 4, 535 (1971).

50. P.H. Stelson, R.L. Robinson, W.T. Milner, F.K. McGowan, and M.A. Ludington, Bull. Am. Phys. Soc. 16, 619 (1971).

51. T. Kammuri, private communication.

52. Program DWUCK, P.D. Kunz, University of Colorado Report COO-535-613 (unpublished).

53. L.R. Dodd and K.R. Greider, Phys. Rev. 180, 1187 (1969).

54. M. Nagarajan, Nucl. Phys. A196, 34 (1972).

55. R.M. DeVries, to be published; R.M. DeVries and K.I. Kubo, Phys. Rev. Letters 30, 325 (1973).

Table I. Calculation of the Favored L-Transfer for the $^{90}Zr \longrightarrow {}^{91}Nb$(g.s.) Transition Using Coulomb Trajectories.

Reaction	E_{lab} (MeV)	$E_{c.m.}$ (MeV)	D[a] (fm)	$V_i^c(D)$ (MeV)	$V_f^c(D)$ (MeV)	Q (MeV)	$k_i(D)$ (fm^{-1})	$k_f(D)$ (fm^{-1})	ℓ_i	ℓ_f	L
(^{16}O,^{15}N)	104	88.3	11.6	39	34	-6.96	5.7	5.4	66	63	3
"	60	50.9	"	"	"	"	2.8	2.5	32	29	3
(α,t)	50	47.9	7.9	16	8	-14.64	2.4	1.9	19	15	4
(^{3}He,d)	31	30.0	7.7	"	"	-0.32	1.4	1.4	11	11	0

[a] $D = d_o (A_1^{1/3} + A_2^{1/3})$. For heavy ions d_o = 1.65 fm, for light ions d_o = 1.3 fm.

Table II. Levels Observed in the $^{90}Zr(^{16}O,^{15}N)^{91}Nb$ and $^{90}Zr(^{12}C,^{11}B)^{91}Nb$ Reactions.

This Work ($^{16}O,^{15}N$) E = 104 MeV			Ref. 2 ($^{16}O,^{15}N$) E = 60 MeV		This Work ($^{12}C,^{11}B$) E = 78 MeV	
Levels Observed[a] (MeV)	Intensity[b] (mb)	Peak Cross Section[c] (mb/sr)	Levels Observed (MeV)	Peak Cross Section[d] (mb/sr)	Levels Observed[e] (MeV)	Peak Cross Section[c] (mb/sr)
0.0[f]	5.30[g]	7.83 ± 0.08[g]	0.0	1.39	0.0[f]	9.29 ± 0.20[g]
1.29	0.20	0.22 ± 0.01			1.27	0.10 ± 0.02
1.60	0.24	0.34 ± 0.02	1.61	0.03	1.58	0.22 ± 0.03
1.88	0.31	0.29 ± 0.02			1.99[h]	1.33 ± 0.07[h]
			2.18	0.04		
					2.26[h]	1.45 ± 0.07[h]
			2.75	0.08		
2.97	0.24	0.34 ± 0.02			2.90	0.25 ± 0.03
3.37[f]	1.66	2.43 ± 0.04	3.36	0.15	3.37	0.78 ± 0.05
4.26	0.32[i]	0.47 ± 0.02			4.22	0.57 ± 0.05
4.81	0.47[i]	0.59 ± 0.02			4.75	1.05 ± 0.06
5.25	0.66[i]	0.94 ± 0.03			5.33	0.93 ± 0.06
5.9 ± 0.15[h]	1.35[h]	1.89 ± 0.04[h]				
6.6 ± 0.15[h]	1.40[h]	2.07 ± 0.04[h]				

(Continued)

Table II. (Continued)

[a]Excitation energy ± 100 keV except as noted.

[b]Integrated from $\theta_{c.m.}$ = 18 to 41° except as noted. The cross sections have been corrected for charge state as described in the text (Sec. II-D).

[c]Differential cross section at θ_{ℓ} = 25°. The error shown is only that due to counting statistics. The cross sections have been corrected for charge state as described in the text (Sec. II-D).

[d]Differential cross section at θ_{ℓ} = 60°.

[e]Excitation energy ± 50 keV.

[f]Used as a calibration point.

[g]Contains a contribution of about 15% from the unresolved 0.10 MeV level.

[h]Probably due to transfer to an excited state of the outgoing particle (see Sec. V-D).

[i]Integrated from $\theta_{c.m.}$ = 18 to 35°.

Table III. Levels Observed in the $^{92}Mo(^{16}O,^{15}N)^{93}Tc$ and $^{92}Mo(^{12}C,^{11}B)^{93}Tc$ Reactions.

This Work $(^{16}O,^{15}N)$ E = 104 MeV		Ref. 27 $(^{16}O,^{15}N)$ E = 66 MeV		This Work $(^{12}C,^{11}B)$ E = 78 MeV	
Levels Observed[a] (MeV)	Peak Cross Section[b] (mb/sr)	Levels Observed (MeV)	Peak Cross Section[c] (mb/sr)	Levels Observed[d] (MeV)	Peak Cross Section[b] (mb/sr)
0.0[e]	4.70 ± 0.19	0.0	0.47 ± 0.05	0.0[e]	5.19 ± 0.15
0.4	0.75 ± 0.08			0.36	0.38 ± 0.04
				2.13[f]	1.66 ± 0.08[f]
2.7	0.23 ± 0.04			2.62	0.21 ± 0.03
3.2	0.37 ± 0.05				
3.36[e]	1.39 ± 0.10	3.36	0.11 ± 0.02	3.37	0.51 ± 0.05
3.8	0.26 ± 0.04			3.87	0.41 ± 0.04
4.4	0.42 ± 0.06				
4.8	0.43 ± 0.06			4.73	0.31 ± 0.04
5.1	0.29 ± 0.05				
5.9[f]	1.39 ± 0.10[f]				
6.7[f]	1.61 ± 0.11[f]				

[a] Absolute energies ± 200 keV, relative energies ± 100 keV.

[b] Differential cross section at $\theta_\ell = 25°$. The error shown is only that due to counting statistics.

(Continued)

Table III. (Continued)

The cross sections have been corrected for charge state as described in the text (Sec. II-D).

[c]Differential cross section at $\theta_\ell = 50°$.

[d]Excitation energy ± 50 keV.

[e]Used as a calibration point.

[f]Probably due to transfer to an excited state of the outgoing particle. (See text, Sec. III-D).

Table IV. Levels Observed in the $^{94}Zr(^{16}O,^{15}N)^{95}Nb$ Reaction.

This Work E = 104 MeV		Ref. 2 E = 60 MeV	
Levels Observed[a] (MeV)	Peak Cross Section[b] (mb/sr)	Levels Observed (MeV)	Peak Cross Section[c] (mb/sr)
0.0[d]	3.24 ± 0.09	0.0	1.43
0.3	0.64 ± 0.04		
0.7	1.12 ± 0.05	0.75 0.92	0.34
1.1	0.17 ± 0.02		
1.5	0.24 ± 0.02		
1.7	0.31 ± 0.03[e]	1.6	0.41
2.0	0.94 ± 0.05	2.05	0.52
3.0	0.40 ± 0.03		
3.2	0.21 ± 0.02		
3.8[f]	1.48 ± 0.06		
4.8[f]	1.56 ± 0.06		
5.9[f]	1.86 ± 0.07		
6.8[f]	1.46 ± 0.06		

[a] Absolute energies ± 200 keV, relative energies ± 100 keV.

[b] Differential cross section at $\theta_\ell = 25°$. The error shown is only that due to counting statistics. The cross sections have been corrected for charge state as described in the text (Sec. II-D).

[c] Differential cross section at $\theta_\ell = 60°$.

[d] Used as a calibration point.

[e] Corrected for $^{90}Zr(^{16}O,^{15}N)^{91}Nb$(g.s.) impurity by about 30%.

[f] Centroids and cross sections are for broad structures (see Fig. 10). Individual levels were not separated.

Table V. Levels Observed in the $^{91}Zr(^{16}O,^{15}N)^{92}Nb$ Reaction at 104 MeV.

Levels Observed[a] (MeV)	Peak Cross Section[b] (mb/sr)
0.4	7.22 ± 0.14
1.8	0.65 ± 0.04
3.6	1.38 ± 0.06
6.3	6.85 ± 0.14

[a]Excitation energy ± 200 keV. All levels are unresolved multiplets.

[b]Differential cross section at $\theta_\ell = 25^\circ$. The error shown is only that due to counting statistics. The cross sections have been corrected for charge state as described in the text (Sec. II-D).

Table VI. Levels Observed in the $^{93}Nb(^{16}O,^{15}N)^{94}Mo$ reaction Compared with Previous Work.

This Work		$^{93}Nb(^{3}He,d)^{94}Mo$[a]			In-beam γ Spectroscopy[b]	
Levels Observed[c] (MeV)	Peak Cross Section[d] (mb/sr)	Levels Observed[e] (MeV)	ℓ_p	J^π	Levels Observed[f] (MeV)	J^π
0.0	0.18 ± 0.02	0.0	4	0^+	(0.0)	0^+
0.9	0.22 ± 0.03	0.873	2,4	2^+	0.870	2^+
1.5	0.10 ± 0.02	1.582	2,4	4^+	1.572	4^+
		1.868	2,4	2^+		
		2.08	4	$(0)^+$		
		2.295	2,4	$(\ )^+$	2.300	
		2.422	2,4	6^+	2.421	6^+
		2.527	1	$(3,4,5,6)^-$		
		2.566	2,4	$(\ )^+$		
2.6	1.22 ± 0.06	2.614	1	$(3,4,5,6)^-$	2.608	5^-
		2.773	2,4	$(\ )^+$	2.738	(4^+)
		2.837	1	$(3,4,5,6)^-$		
2.9	2.71 ± 0.09	2.875	4	$(8)^+$	2.870	$6^{(\pm)}$[g]
		2.960	4	$(8,1)^+$	2.953	$8^{(\pm)}$[g]
		3.026	1	$(3,4,5,6)^-$		

(Continued)

Table VI. (Continued)

This Work		$^{93}Nb(^{3}He,d)^{94}Mo$[a]			In-beam γ Spectroscopy[b]	
Levels Observed[c] (MeV)	Peak Cross Section[d] (mb/sr)	Levels Observed[e] (MeV)	ℓ_p	J^π	Levels Observed[f] (MeV)	J^π
					3.318	(8 to 10)
					3.357	(8^+)
					3.364	(7^-)
					3.803	(9 to 12)
					3.865	
					3.894	$10^{(\pm)}$[g]
					4.005	(8 to 10)
4.1	0.54 ± 0.04				4.187	(11,12)
					4.493	(8 to 10)
8.8[h]	1.53 ± 0.07					
9.9[h]	1.20 ± 0.06					

[a] Ref. 7. [b] Ref. 30. [c] Absolute energies ± 200 keV, relative energies ± 100 keV.

[d] Differential cross section at $\theta_\ell = 25°$. The error shown is only that due to counting statistics. The cross sections have been corrected for charge state as described in the text (Sec. II-D).

[e] Excitation energy ± 5 keV. [f] Excitation energy ± 1 keV.

(Continued)

Table VI. (Continued)

[g]The 2.870, 2.953, and 3.894 MeV states are connected by E2 decay and must all have the same parity.

[h]Centroids and cross sections are for broad structures (see Fig. 12). Individual levels were not separated.

Table VII. Levels Observed in the $^{90}Zr(^{16}O,^{15}O)^{91}Zr$ Reaction Compared with Previous Work.

This Work				$^{90}Zr(d,p)^{91}Zr$[a]			$^{90}Zr(\alpha,^{3}He)^{91}Zr$[a]	
Levels Observed[b] (MeV)	Peak Cross Section[c] (mb/sr)	J^{π}[d]	θ_2^0[d]	Levels Observed (MeV)	J^{π}	C^2S	Levels Observed (MeV)	C^2S
0.0[e]	3.07 ± 0.06	$5/2^+$	1.0[f]	0.0	$5/2^+$	1.04	0.0	0.98
				1.201	$1/2^+$	0.93		
				1.459	$5/2^+$	0.03		
				1.871	$7/2^+$	0.08	1.874	0.09
				2.031	$3/2^+$	0.63	2.040	0.45
2.16[e]	3.38 ± 0.06	$11/2^-$	0.91	2.157	$11/2^-$	0.37	2.176	0.41
				2.186	$7/2^+$	0.48		0.48
				2.309	$11/2^-$	0.05	2.323	0.05
				2.541	$1/2^+$	0.34		
2.7	0.12 ± 0.01	$5/2^+$ $3/2^+$	0.48 39.[g]	2.681				
				2.792	$(3/2^+)$[h] $5/2^+$	0.07[h] 0.03		
				2.853	$3/2^+$	0.08	2.847	0.13
				2.902	$(1/2^+)$	0.10		
				2.992				
				3.068	$3/2^+$	0.28	3.063	0.22

(Continued)

Table VII. (Continued)

This Work				$^{90}Zr(d,p)^{91}Zr$[a]			$^{90}Zr(\alpha,{}^{3}He)^{91}Zr$[a]	
Levels Observed[b] (MeV)	Peak Cross Section[c] (mb/sr)	J^{π}[d]	$\mathcal{D}_2$[d]	Levels Observed (MeV)	J^{π}	C^2S	Levels Observed (MeV)	C^2S
				3.270	$3/2^+$	0.17	3.277	0.19
3.4	0.31 ± 0.02	$7/2^+$	335.[g]	3.444	$7/2^+$	0.42	3.466	0.34
				3.533	$7/2^+$	0.09	3.575	0.08
				3.610				
				3.661	$(3/2^+)$ $(11/2^-)$	(0.11) (0.03)	3.676	(0.11) (0.03)
				3.721				
				3.824	$(3/2^+)$	0.12	3.817	0.19
3.8	0.29 ± 0.02	$3/2^+$ $11/2^-$	117.[g] 0.16	3.880	$(3/2^+)$ $(11/2^-)$	(0.05) (0.08)	3.904	(0.05) (0.09)
4.1	0.11 ± 0.01	$11/2^-$	0.06		$11/2^-$		4.081	0.04
					$11/2^-$		4.254	0.06
4.4	0.12 ± 0.01	$11/2^-$	0.07					
4.7	0.12 ± 0.01	$11/2^-$	0.08					
5.0	0.15 ± 0.01	$11/2^-$	0.09					

(Continued)

Table VII. (Continued)

[a] Ref. 36

[b] Absolute energies ± 200 keV, relative energies ± 100 keV.

[c] Differential cross section at $\theta_\ell = 25°$. The error shown is only that due to counting statistics.

[d] The spin and parity assumed for the DWBA calculations and the spectroscopic factor deduced under that assumption. The J^π are not determined in the present experiment. The potentials used are given in Table XIV, footnote (a).

[e] Used as a calibration point.

[f] The DWBA calculations have been normalized such that $\mathcal{S}_2 = 1.0$ for the ^{91}Zr(g.s.) transition.

[g] $\mathcal{S}_2$ for states with $j_2 = \ell_2 - 1/2$ is deduced using the no-recoil selection rules, Eqs. (9)-(11). See Sec. V-C.

[h] Ref. 35.

Table VIII. Levels Observed in the $^{92}Mo(^{16}O,^{15}O)^{93}Mo$ Reaction Compared with Previous Work.

This Work				$^{92}Mo(d,p)^{93}Mo$[a]		
Levels Observed[b] (MeV)	Peak Cross Section[c] (mb/sr)	J^π[d]	ℓ_2[d]	Levels Observed[e] (MeV)	J^π	C^2S
0.0[f]	2.64 ± 0.11	$5/2^+$	0.69	0.0	$5/2^+$	0.87
0.9	0.05 ± 0.02	$1/2^+$	0.25	0.950	$1/2^+$	0.64
1.3	0.22 ± 0.03	$7/2^+$	6.8[g]	1.371	$7/2^+$	0.26
		$9/2^+$	0.05	1.486[h]	$9/2^+$	
1.5	0.48 ± 0.05	$3/2^+$	32.[g]	1.502	$3/2^+$	0.50
		$7/2^+$	15.[g]	1.529	$7/2^+$	0.14
		$9/2^+$	0.11			
				1.706	$3/2^+$	0.18
				2.157	$1/2^+$	0.007
				2.194	$3/2^+$	0.053
2.32[f]	2.50 ± 0.11	$11/2^-$	0.67	2.320	$11/2^-$	0.33

[a]Refs. 39 and 40. [b]Absolute energies ± 200 keV, relative energies ± 100 keV.

[c]Differential cross section at $\theta_\ell = 25°$. The error shown is only that due to counting statistics.

[d]The spin and parity assumed for the DWBA calculations and the spectroscopic factor deduced under that assumption. The DWBA normalization, etc., are the same as for Table VII.

(Continued)

Table VIII. (Continued)

[e] Only levels below 2.32 MeV are included.

[f] Used as a calibration point.

[g] See text, Sec. V-C.

[h] Observed only in the ^{94}Mo(d,t) data of Ref. 40.

Table IX. Levels Observed in the $^{93}Nb(^{16}O,^{15}O)^{94}Nb$ Reaction at 104 MeV.

Levels Observed[a] (MeV)	Adjusted Energy[b] (MeV)	Peak Cross Section[c] (mb/sr)
-0.05	0.06	1.68± 0.06
1.8	1.91	1.23± 0.05
2.2	2.31	0.96± 0.04

[a] Excitation energy ± 200 keV.

[b] Normalized to the expected excitation energy of the low-lying $[\pi g_{9/2},(\nu d_{5/2})^3_{5/2}]$ multiplet. See text, Sec. III-K.

[c] Differential cross section at $\theta_\ell = 25^\circ$. The error shown is only that due to counting statistics.

Table X. Levels Observed in the $^{94}Zr(^{16}O,^{15}O)^{95}Zr$ Reaction at 104 MeV.

Levels Observed[a] (MeV)	Peak Cross Section[b] (uncorrected) (mb/sr)	Peak Cross Section[c] (corrected) (mb/sr)	J^{π}[d]	$\mathcal{S}_2$[d]
0.0	0.16 ± 0.02	0.87 ± 0.44	$5/2^+$	0.47
2.0	0.14 ± 0.02	0.72 ± 0.36	$11/2^-$	0.23

[a] Excitation energy ± 200 keV.

[b] $^{15}O(7+)$ differential cross section at $\theta_\ell = 25^\circ$, but calculated as for $^{15}O(8+)$. See Sec. II-D, Eq. (8b). The error shown is only that due to counting statistics.

[c] $^{15}O(7+)$ cross section from column 2 after correction by $R_{8/7}$ from Sec. II-D, Eq. (4b). An arbitrary error of ± 50% is assumed for the correction.

[d] The spin and parity assumed for the DWBA calculations and the spectroscopic factor deduced under that assumption. The DWBA normalization, etc., are the same as for Table VII.

Table XI. Levels Observed in the $^{91}Zr(^{16}O,^{15}O)^{92}Zr$ Reaction at 104 MeV.

Levels Observed[a] (MeV)	Peak Cross Section[b] (uncorrected) (mb/sr)	Peak Cross Section[c] (corrected) (mb/sr)
0.9	0.20 ± 0.02	1.13 ± 0.67
1.5	0.37 ± 0.03	2.03 ± 1.02
3.5	0.21 ± 0.02	1.11 ± 0.56

[a] Excitation energy ± 200 keV.

[b] $^{15}O(7+)$ differential cross section at $\theta_\ell = 25^\circ$, but calculated as for $^{15}O(8+)$. See Sec. II-D, Eq. (8b). The error shown is only that due to counting statistics.

[c] $^{15}O(7+)$ cross section from column 2 after correction by $R_{8/7}$ from Sec. II-D, Eq. (4b). An arbitrary error of ± 50% is assumed for the correction.

Table XII. $Zr(^{16}O,^{17}O)$ Cross Sections at 104 MeV.

Reaction[b]	Peak Cross Section[a] (mb/sr) Target: ^{90}Zr	^{91}Zr	^{94}Zr
$^{91}Zr(^{16}O,^{17}O)^{90}Zr(g.s.)$	12.6 ± 1.0	12.4 ± 0.2	——
$^{91}Zr(^{16}O,^{17}O^{*})^{90}Zr(g.s.)$	——	2.8 ± 0.1	——
$^{92}Zr(^{16}O,^{17}O)^{91}Zr(g.s.)$	12.1 ± 1.2	——	——
$^{94}Zr(^{16}O,^{17}O)^{93}Zr(g.s.)$	20.5 ± 1.8	——	21.8 ± 0.2
$^{96}Zr(^{16}O,^{17}O)^{95}Zr(g.s.)$	(51. ± 6.)[c]	——	——

[a]Differential cross section at $\theta_{\ell} = 25^{o}$. Isotopic abundances are taken from Ref. 4. The error shown is only that due to counting statistics.

[b]The "$^{17}O^{*}$" refers to the outgoing ^{17}O being in its 0.87 MeV ($s_{1/2}$) first excited state.

[c]The amount of ^{96}Zr is given as < 0.1%, so only a lower limit to the cross section can be calculated.

Table XIII. Collective Levels Observed in Zr(^{16}O,^{15}N)Nb Compared with Zr(α,t)Nb Results.

Target	(^{16}O,^{15}N)[a]		(α,t)[b]		(^{16}O,^{15}N)[a]		(α,t)[b]	
	E_2[c] (MeV)	I_2[d]	E (MeV)	I[e]	E_3[f] (MeV)	I_3[d]	E (MeV)	I[e]
^{90}Zr	2.18	0.03	2.30	0.01	2.75	0.06	2.61	0.007
							2.77	0.003
							2.90	0.02
^{92}Zr	0.93	0.05	0.95	0.02	2.34	0.17	2.30, 2.36	0.03
^{94}Zr	0.92	——	0.82	0.04	2.05	0.36	2.10	0.08
			1.00	0.01				

[a] Taken from Ref. 2.

[b] Taken from Refs. 3 and 4.

[c] Assumed [Zr(2^+) ⊗ $\pi g_{9/2}$] configuration.

[d] Ratio of differential cross section (at $\theta_\ell = 60°$) to that of ground state.

[e] Ratio of integrated cross section to that of ground state.

[f] Assumed [Zr(3^-) ⊗ $\pi g_{9/2}$] configuration.

Table XIV. Spectroscopic Factors for ^{91}Nb Levels.

This Work[a] (^{16}O,^{15}N) E(^{16}O) = 104 MeV				This Work[a] (^{12}C,^{11}B) E(^{12}C) = 78 MeV				Refs. 7 and 44 (^{3}He,d) E(^{3}He) = 31 MeV		
E_x[b] (MeV)	J^π[c]	L[d]	$\mathcal{S}_2$[e]	E_x[b] (MeV)	J^π[c]	L[d]	$\mathcal{S}_2$[e]	E_x[f] (MeV)	ℓ_p[f]	C^2S[f]
0.0	$9/2^+$	5	1.0[g]	0.0	$9/2^+$	3,5	1.0[g]	0.0	4	0.92
								0.10	1	0.43
1.29	$3/2^-$	2	0.06	1.27	$3/2^-$	0,2	0.05	1.31	1	0.05
1.60	$3/2^-$	2	0.09	1.58	$3/2^-$	0,2	0.11	1.60	1	0.08
1.88	$5/2^-$	2	1.56[h]	----				1.84	3	0.06
2.97	$5/2^+$	3	0.04[h]	2.90	$5/2^+$	1,3	0.11	3.07	2	0.04
	$3/2^+$	1	2.17[h]		$3/2^+$	1,3	0.06	3.11		
3.37	$5/2^+$	3	0.33	3.37	$5/2^+$	1,3	0.33	3.36	2	0.39
4.26	$5/2^+$	3	0.07[h]	4.22	$5/2^+$	1,3	0.30	4.18	2	0.05
	$3/2^+$	1	5.3[h]		$3/2^+$	1,3	0.17	to 4.30		
	$9/2^+$	5	0.1[h]		$9/2^+$	3,5	0.3			
	$7/2^+$	3	6.9[h]		$7/2^+$	3,5	0.12			
	$11/2^-$	6	0.05		$11/2^-$	4,6	0.11			
4.81	$9/2^+$	5	0.12[h]	4.75	$9/2^+$	3,5	0.55	4.77	4	0.34
	$7/2^+$	3	10.0[h]		$7/2^+$	3,5	0.23	4.80		
	$11/2^-$	6	0.08		$11/2^-$	4,6	0.25			
5.25	$5/2^+$	3	0.13[h]	5.33	$5/2^+$	1,3	0.49	5.24	2	0.13
	$3/2^+$	1	9.0[h]		$3/2^+$	1,3	0.27			

(Continued)

Table XIV. (Continued)

[a]The Woods-Saxon potentials used in the calculations are: i) Optical Potential: V= -40 MeV, W= -15 MeV, R= $1.30(A_1^{1/3} + A_2^{1/3})$ fm, and a= 0.5 fm; ii) Proton and neutron bound states in the projectile: R= $1.20\ A_1^{1/3}$ fm, a= 0.65 fm, λ_{SO}= 0, and V adjusted to fit the binding energy; iii) Proton states in the final nucleus: R= $1.28\ A_2^{1/3}$ fm, a= 0.76 fm, λ_{SO}= 18, and V adjusted (C.J. Batty and G.W. Greenlees, Nucl. Phys. A133, 673 (1969)); iv) Neutron states in the final nucleus: R= $1.25\ A_2^{1/3}$ fm, a= 0.70 fm, λ_{SO}= 18, and V adjusted.

[b]From Table II.

[c]Spin and parity of the final state assumed for the DWBA calculations.

[d]From Eqs. (9)-(11).

[e]Spectroscopic factor ($\mathcal{S}_2 \equiv C^2S_2$) deduced from DWBA calculations for the assumed J^π, normalized to θ_ℓ= 25°.

[f]Excitation energy ± 15 keV. All ℓ_p= 2 levels assumed $d_{5/2}$, all ℓ_p= 1 levels except 0.10 MeV assumed $p_{3/2}$, all ℓ_p= 4 levels except g.s. assumed $g_{7/2}$, all ℓ_p= 3 levels assumed $f_{5/2}$. Only levels near those seen in the heavy ion data are listed.

[g]The DWBA results are normalized such that $\mathcal{S}_2$= 1.0 for the ^{91}Nb g.s.

[h]See Sec. V-C for a discussion of $\mathcal{S}_2$ determined for states with $j_2=\ell_2-1/2$.

Table XV. Spectroscopic Factors for ^{93}Tc Levels.

This Work[a] (^{16}O,^{15}N) E(^{16}O) = 104 MeV				This Work[a] (^{12}C,^{11}B) E(^{12}C) = 78 MeV				Ref. 49 (^{3}He,d) E(^{3}He) = 35 MeV		
E_x[b] (MeV)	J^π[c]	L[d]	$\mathcal{S}_2$[e]	E_x[b] (MeV)	J^π[c]	L[d]	$\mathcal{S}_2$[e]	E_x[f] (MeV)	ℓ_p[g]	C^2S[g]
0.0	$9/2^+$	5	0.49	0.0	$9/2^+$	3,5	0.56	0.0	4	0.50
0.4	$1/2^-$	0	4.78[h]	0.36	$1/2^-$	2	0.09	0.40	1	0.28
2.7	$5/2^+$	3	0.04[h]	2.62	$5/2^+$	1,3	0.08	2.56	2	0.019
	$3/2^+$	1	1.57[h]		$3/2^+$	1,3	0.03			0.037
3.2	$5/2^+$	3	0.07[h]	---				3.15	2	0.018
	$3/2^+$	1	2.90[h]							0.034
3.36	$5/2^+$	3	0.28[h]	3.37	$5/2^+$	1,3	0.43	3.34	2	0.41
	$3/2^+$	1	11.8[h]		$3/2^+$	1,3	0.21			0.78
3.8	$5/2^+$	3	0.07[h]	3.87	$5/2^+$	1,3	0.25	3.89	(2)	(0.06)
	$3/2^+$	1	2.95[h]		$3/2^+$	1,3	0.11			(0.11)
	$9/2^+$	5	0.03[h]		$9/2^+$	3,5	0.10			
	$7/2^+$	3	3.4[h]		$7/2^+$	3,5	0.06			
	$11/2^-$	6	0.03		$11/2^-$	4,6	0.07			
4.4	$5/2^+$	3	0.14[h]					4.39		
	$3/2^+$	1	5.72[h]							
	$9/2^+$	5	0.06[h]							
	$7/2^+$	3	6.0[h]							
	$11/2^-$	6	0.05							

(Continued)

Table XV. (Continued)

This Work[a] (^{16}O,^{15}N) $E(^{16}O)$ = 104 MeV				This Work[a] (^{12}C,^{11}B) $E(^{12}C)$ = 78 MeV				Ref. 49 (^{3}He,d) $E(^{3}He)$ = 35 MeV		
E_x[b] (MeV)	J^{π}[c]	L[d]	$\mathcal{S}_2$[e]	E_x[b] (MeV)	J^{π}[c]	L[d]	$\mathcal{S}_2$[e]	E_x[f] (MeV)	ℓ_p[g]	C^2S[g]
4.8	$5/2^+$	3	0.15[h]	4.73	$5/2^+$	1,3	0.65	{4.76		
	$3/2^+$	1	6.27[h]		$3/2^+$	1,3	0.30	{4.88		
	$9/2^+$	5	0.07[h]		$9/2^+$	3,5	0.14			
	$7/2^+$	3	7.2[h]		$7/2^+$	3,5	0.08			
	$11/2^-$	6	0.05		$11/2^-$	4,6	0.10			
5.1	$3/2^-$	2	0.46[h]	5.10	$3/2^-$	0,2	<0.8	5.17	1	0.083
	$1/2^-$	0	26.0[h]		$1/2^-$	2	<1.5			0.23

[a] See Table XIV, footnote (a).

[b] See Table III.

[c] Spin and parity of the final state assumed for the DWBA calculations.

[d] From Eqs. (9)-(11).

[e] Spectroscopic factor ($\mathcal{S}_2 \equiv C^2S_2$) deduced from DWBA calculations for the assumed J^{π}, normalized to $\theta_\ell = 25^{\circ}$.

[f] Excitation energies ± 40 keV or less.

[g] When two values are listed the upper corresponds to $j_2=\ell_2+1/2$, the lower to $j_2=\ell_2-1/2$. For light ion transfer reactions, $\ell_p=\ell_2$ in both cases.

[h] See Sec. V-C for a discussion of $\mathcal{S}_2$ determined for states with $j_2=\ell_2-1/2$.

Table XVI. Projectile Spectroscopic Factors.

Reaction	$E_x(1)$[a] (MeV)	$E_x(2)$[b] (MeV)	$(n\ell j)_1$[c]	$(n\ell j)_2$[d]	$\mathcal{S}_1$[e] This Work	$\mathcal{S}_1$[f] Pickup
$^{90}Zr(^{16}O,^{15}N)^{91}Nb$	0	0	$1p_{1/2}$	$1g_{9/2}$	2.14[g]	2.14[h]
$^{90}Zr(^{16}O,^{15}N)^{91}Nb$	6	0	$1p_{3/2}$	$1g_{9/2}$	2.49[i]	3.72[h]
$^{94}Zr(^{16}O,^{15}N)^{95}Nb$	6	0	$1p_{3/2}$	$1g_{9/2}$	3.01[i]	3.72[h]
$^{92}Mo(^{16}O,^{15}N)^{93}Tc$	6	0	$1p_{3/2}$	$1g_{9/2}$	2.79[i]	3.72[h]
$^{90}Zr(^{12}C,^{11}B)^{91}Nb$	0	0	$1p_{3/2}$	$1g_{9/2}$	2.98[g] 10.4[i,j]	2.98[k]
$^{90}Zr(^{12}C,^{11}B)^{91}Nb$	2	0	$1p_{1/2}$	$1g_{9/2}$	1.19[ℓ]	0.78[k]
$^{92}Mo(^{12}C,^{11}B)^{93}Tc$	2	0	$1p_{1/2}$	$1g_{9/2}$	1.94[ℓ]	0.78[k]
$^{90}Zr(^{16}O,^{15}O)^{91}Zr$	0	0	$1p_{1/2}$	$2d_{5/2}$	3.32[i,j]	1.8[m]

[a] Excitation energy of projectile. [b] Excitation energy of final nucleus.

[c] Assumed nℓj values for nucleon transferred from projectile.

[d] Assumed nℓj values for nucleon transferred to target.

[e] Deduced from DWBA calculations. The various potentials are given in Table XIV, footnote (a).

[f] Deduced from light ion pickup reactions.

[g] Normalized to the light ion result.

[h] J.C. Hiebert, E. Newman, and R.H. Bassel, Phys. Rev. 154,898 (1967).

[i] Obtained with the normalization constant determined from the $^{90}Zr(^{16}O,^{15}N)^{91}Nb$ reaction with $E_x(1)$= 0 MeV and $E_x(2)$= 0 MeV.

[j] Deduced from cross section ratio to $^{90}Zr(^{16}O,^{15}N)$ assuming $\mathcal{S}_2 = 1$.

[k] F. Hinterberger, G. Mairle, U. Schmidt-Rohr, P. Turek, and G.J. Wagner, Nucl. Phys. A106, 161 (1968).

[ℓ] Obtained with the normalization constant determined from the $^{90}Zr(^{12}C,^{11}B)^{91}Nb$ reaction with $E_x(1)$ = 0 MeV and $E_x(2)$ = 0 MeV.

[m] J.L. Snelgrove and E. Kashy, Phys. Rev. 187, 1246 (1969).

FIGURE CAPTIONS

Fig. 1. Schematic diagram of the 24-inch scattering chamber and magnetic spectrometer.

Fig. 2. Simplified block diagram of the electronics used in conjunction with the heavy ion focal plane detector system.

Fig. 3. Corrected time-of-flight vs position spectrum obtained from the bombardment of ^{90}Zr with 104 MeV ^{16}O at $\theta_\ell = 25°$. The M/q value for each band of particles is indicated at the right of the figure. A display threshold of 10 counts was used to clearly differentiate the various bands. The dots are intensified on a logarithmic scale.

Fig. 4. $\Delta E/\Delta X$ vs position spectrum obtained from the bombardment of ^{90}Zr with 104 MeV ^{16}O at $\theta_\ell = 25°$. Bands corresponding to carbon, nitrogen, and oxygen are indicated at the right of the figure. A display threshold of 10 counts was employed. The dots are intensified on a logarithmic scale.

Fig. 5. Time-of-flight vs $\Delta E/\Delta X$ spectrum obtained from the bombardment of ^{90}Zr with 104 MeV ^{16}O at $\theta_\ell = 25°$. The TOF signals were corrected by the computer (see Fig. 3) to remove the position dependence. Groups corresponding to various values of M/q and Z are indicated. A display threshold of 15 counts was employed. The dots are intensified on a logarithmic scale.

Fig. 6. Top: ^{15}N position spectrum from the $^{90}Zr(^{16}O,^{15}N)^{91}Nb$ reaction at $\theta_\ell = 25°$. The two-dimensional arrays corresponding to this spectrum are displayed in Figs. 3 to 5.

Bottom: ^{11}B position spectrum from the $^{90}Zr(^{12}C,^{11}B)^{91}Nb$ reaction at $\theta_\ell = 25°$. The edge of the detector occurs at about channel 15, as shown.

Fig. 7. Angular distributions of ^{15}N from the $^{90}Zr(^{16}O,^{15}N)^{91}Nb$ reaction leading to the 0.0 MeV ($g_{9/2}$) and 3.37 MeV ($d_{5/2}$) states. The curves are DWBA calculations for the angular momentum transfers indicated (see Sec. V).

Fig. 8. Position spectra from the inelastic scattering of 104 MeV ^{16}O on targets of ^{90}Zr, ^{92}Mo, and ^{93}Nb. The broad groups near 6 MeV are probably due to (Doppler broadened) ^{16}O excited states.

Fig. 9. Top: ^{15}N position spectrum from the $^{92}Mo(^{16}O,^{15}N)^{93}Tc$ reaction at $\theta_\ell = 20°$.
Bottom: ^{11}B position spectrum from the $^{92}Mo(^{12}C,^{11}B)^{93}Tc$ reaction at $\theta_\ell = 25°$. The position of the $^{11}B^*(p_{1/2})$ state is indicated. The edge of the detector occurs at about channel 15, as shown.

Fig. 10. ^{15}N position spectrum from the $^{94}Zr(^{16}O,^{15}N)^{95}Nb$ reaction at $\theta_\ell = 25°$.

Fig. 11. ^{15}N position spectrum from the $^{91}Zr(^{16}O,^{15}N)^{92}Nb$ reaction at $\theta_\ell = 25°$. The peak near channel 50 is due to leak-through of an intense ^{17}O peak from the $^{15}O(7+)$ gate (see Fig. 17).

Fig. 12. ^{15}N position spectrum from the $^{93}Nb(^{16}O,^{15}N)^{94}Mo$ reaction at $\theta_\ell = 20°$.

Fig. 13. ^{15}O position spectrum from the $^{90}Zr(^{16}O,^{15}O)^{91}Zr$ reaction at $\theta_\ell = 25°$. A $^{90}Zr(\alpha,^3He)^{91}Zr$ spectrum at $\theta_\ell = 25°$ is shown for comparison.

Fig. 14. ^{15}O angular distributions from the $^{90}Zr(^{16}O,^{15}O)^{91}Zr$ reaction leading to the 0.0 MeV ($d_{5/2}$) and 2.16 MeV ($h_{11/2}$) states. According to the selection rules the ground state transition is L=3 and the 2.16 MeV transition is L=6. The curves are DWBA calculations (see Sec. V).

Fig. 15. ^{15}O position spectrum from the $^{92}Mo(^{16}O,^{15}O)^{93}Mo$ reaction at $\theta_\ell = 20°$. A $^{92}Mo(\alpha,^3He)^{93}Mo$ spectrum at $\theta_\ell = 25°$ is shown for comparison.

Fig. 16. ^{15}O position spectrum from the $^{93}Nb(^{16}O,^{15}O)^{94}Nb$ reaction at $\theta_\ell = 20°$. The calculated energy of the $[\pi g_{9/2},(\nu d_{5/2})^3_{5/2}]$ multiplet was found to be -0.05 MeV. The excitation energies for all three states are believed to be low by about 110 keV. (See text, Sec. III-K.)

Fig. 17. Top: $^{15}O(7+)$ position spectrum from the $^{90}Zr(^{16}O,^{15}O)^{91}Zr$ reaction at $\theta_\ell = 25°$. The small peaks near channel 50 are due to $^{17}O(8+)$ from the $(^{16}O,^{17}O)$ reaction on isotopic impurities in the target leading to the final states indicated above the peaks.

Middle: $^{15}O(7+)$ position spectrum from the $^{91}Zr(^{16}O,^{15}O)^{92}Zr$ reaction at $\theta_\ell = 25°$. The peaks at the bottom of the spectrum are due to the $^{91}Zr(^{16}O,^{17}O)^{90}Zr$ (g.s.) reaction, with the larger one being due to ^{17}O in its ground state and the smaller one to ^{17}O in its 0.87 MeV ($s_{1/2}$) first excited state.

Bottom: $^{15}O(7+)$ position spectrum from the $^{94}Zr(^{16}O,^{15}O)^{95}Zr$ reaction at $\theta_\ell = 25°$. The large peak at the bottom of the spectrum is due to the $^{94}Zr(^{16}O,^{17}O)^{93}Zr$ (g.s.) reaction.

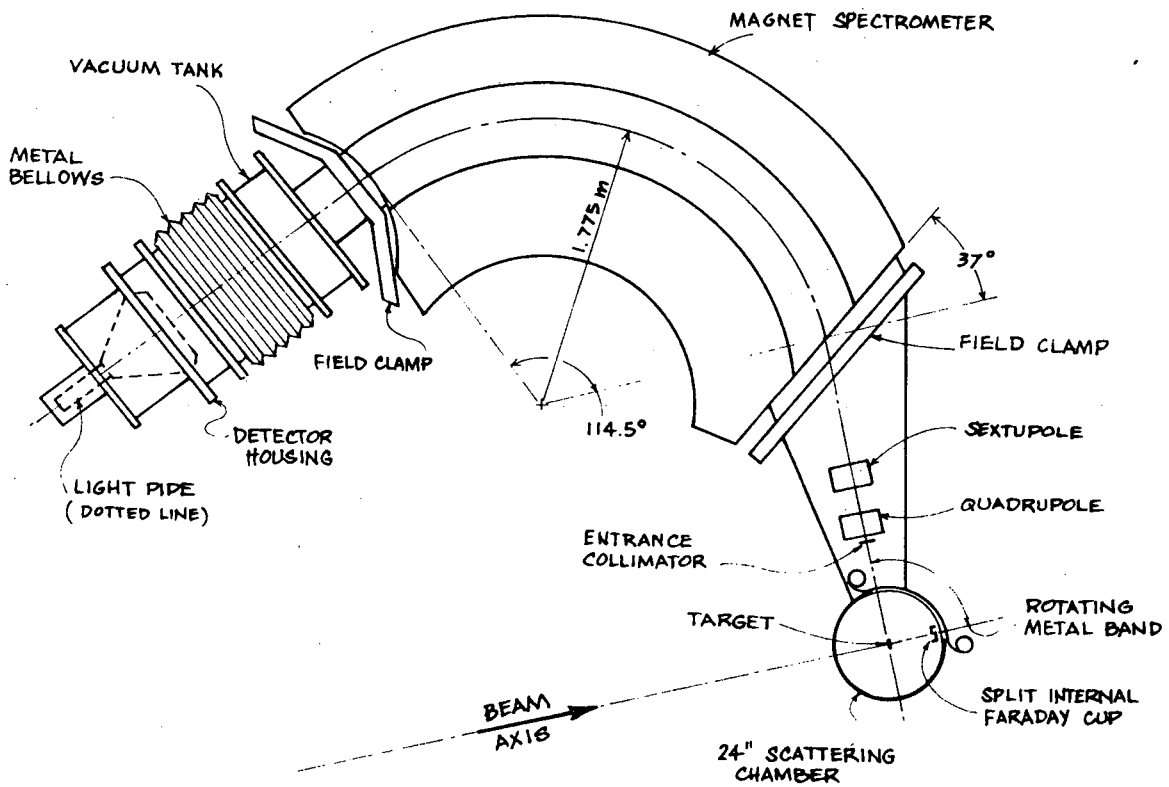
MAGNET SPECTROMETER
VACUUM TANK
METAL BELLOWS
1.775 m
37°
FIELD CLAMP
FIELD CLAMP
114.5°
DETECTOR HOUSING
SEXTUPOLE
LIGHT PIPE (DOTTED LINE)
QUADRUPOLE
ENTRANCE COLLIMATOR
TARGET
ROTATING METAL BAND
BEAM AXIS
SPLIT INTERNAL FARADAY CUP
24" SCATTERING CHAMBER
XBL 726-1074

Fig. 1

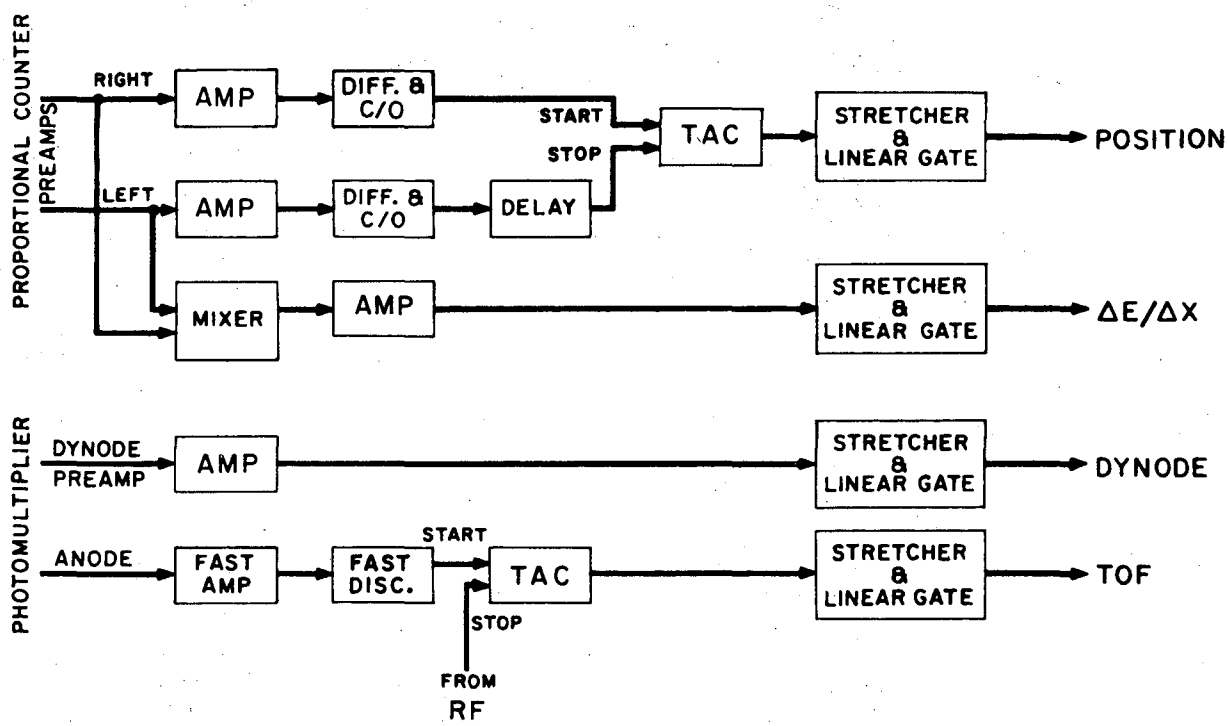

XBL 733-277

Fig. 2

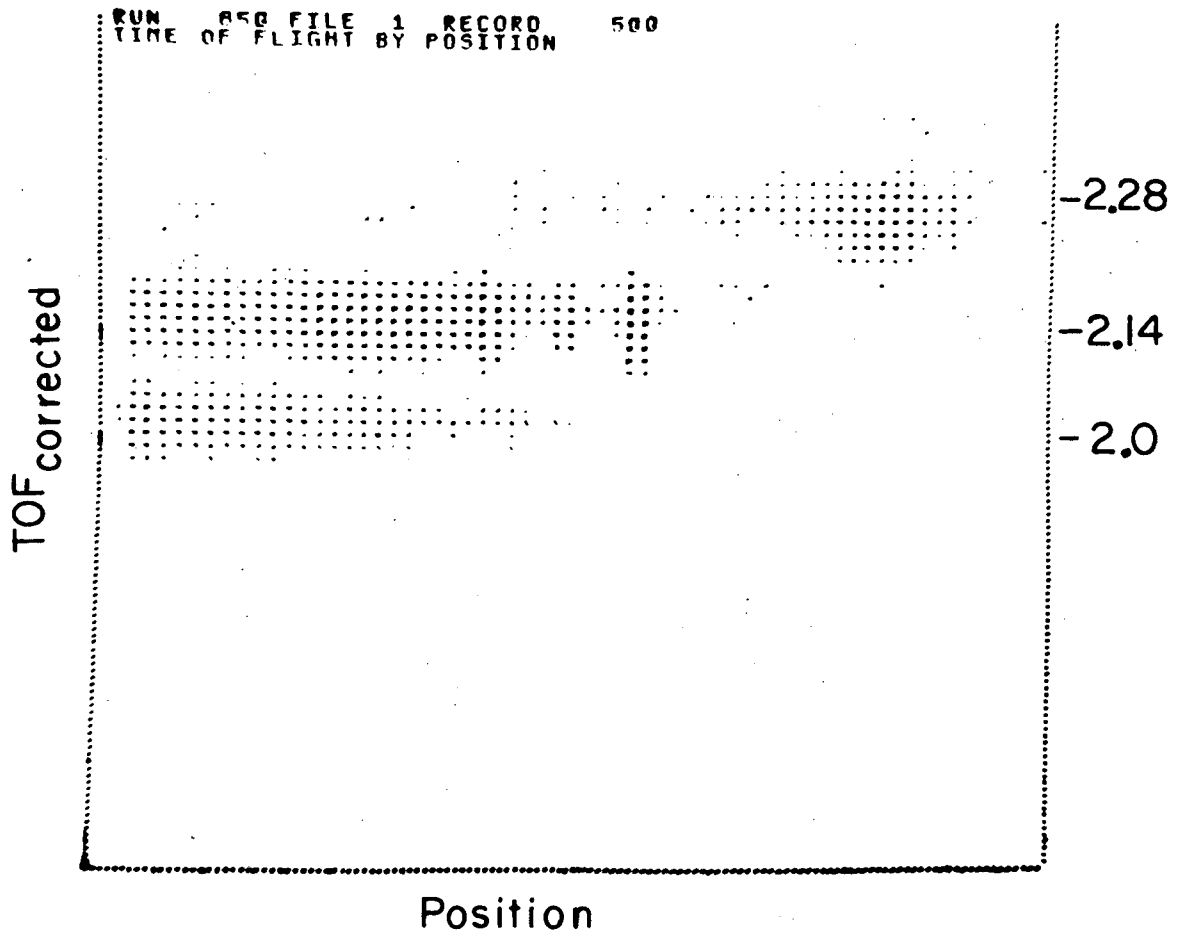
RUN 858 FILE 1 RECORD 500
TIME OF FLIGHT BY POSITION
TOF corrected
-2.28
-2.14
-2.0
Position

Fig. 3

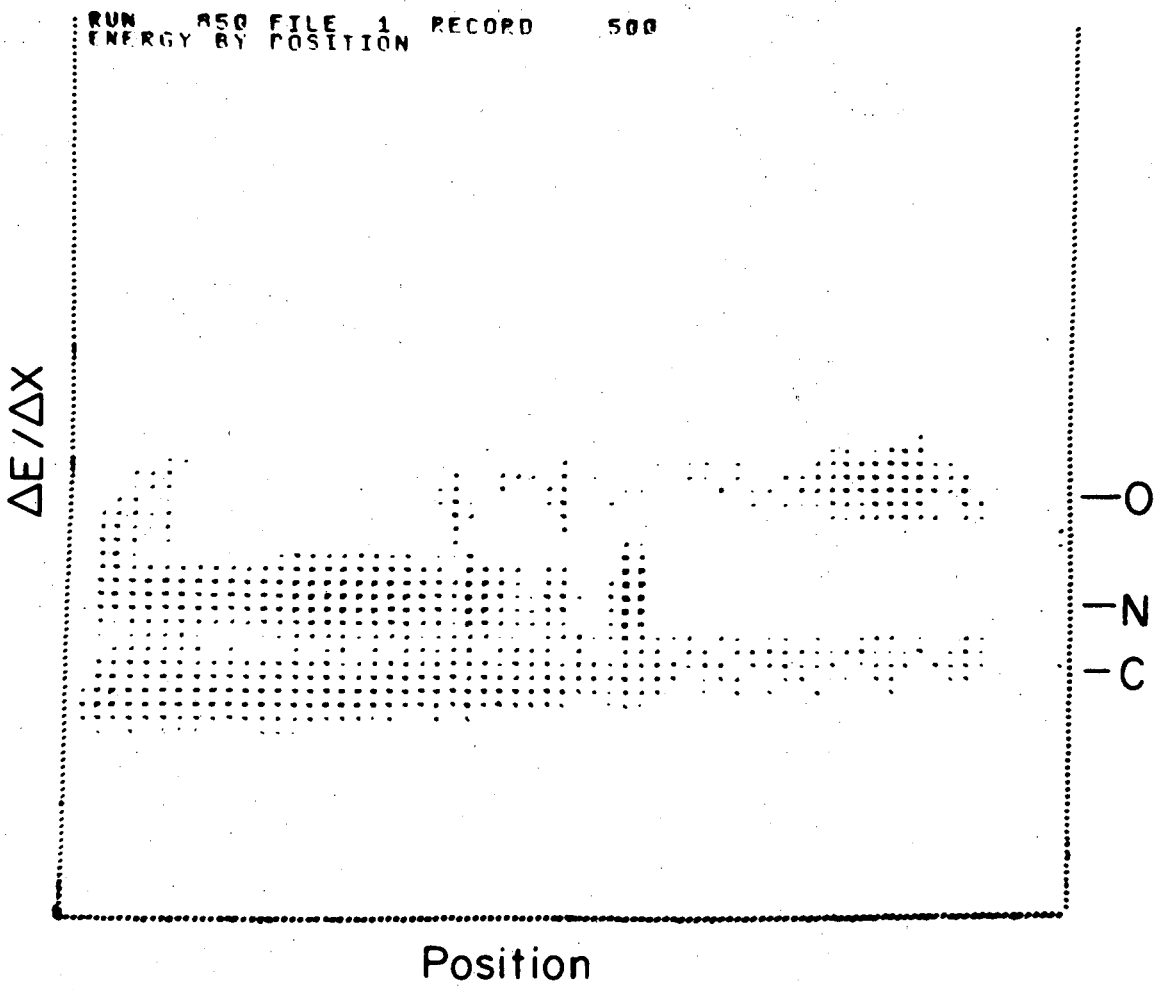
RUN 850 FILE 1 RECORD 500
ENERGY BY POSITION
ΔE/ΔX
Position
O
N
C

Fig. 4

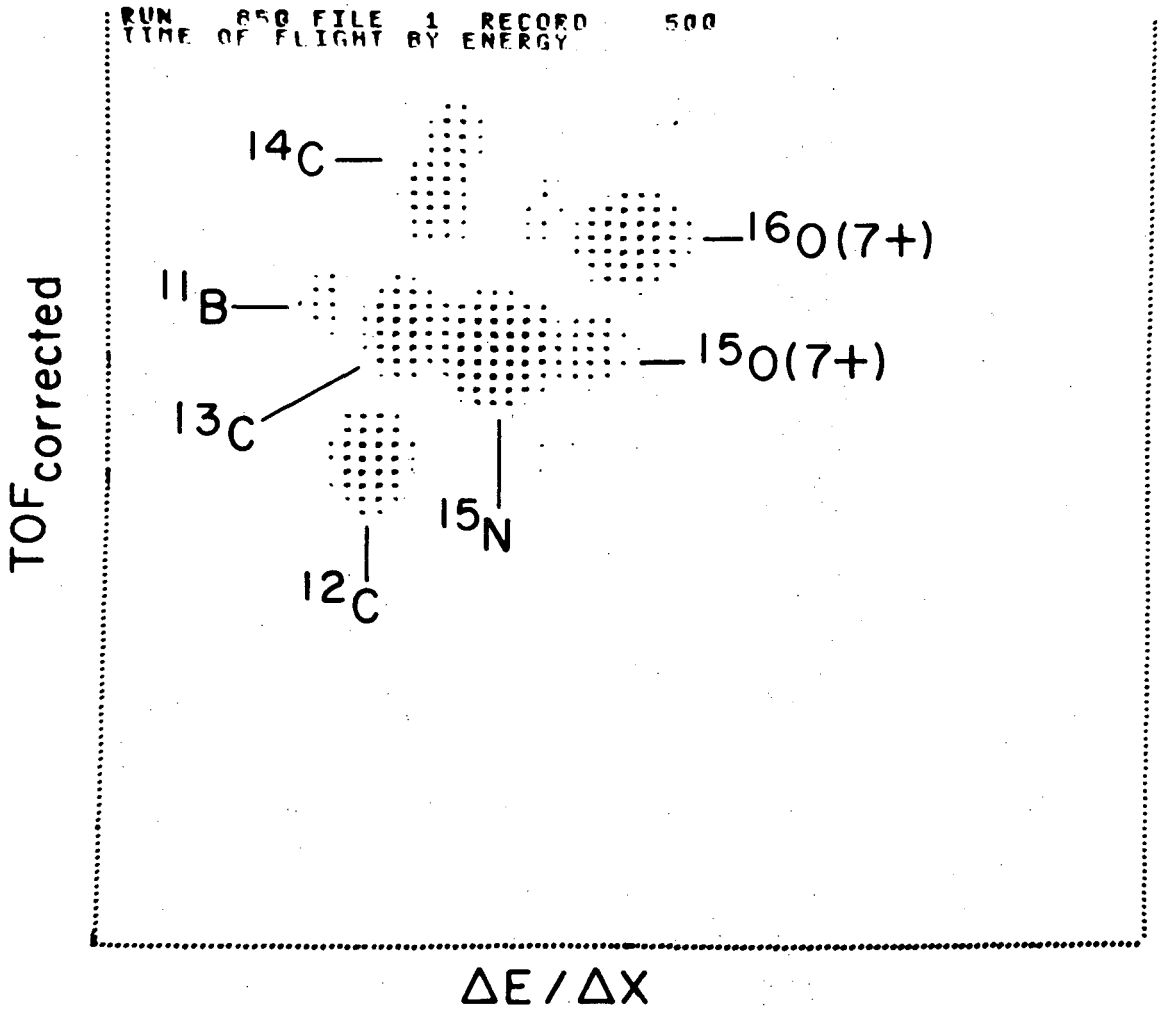
RUN 850 FILE 1 RECORD 500
TIME OF FLIGHT BY ENERGY
14C
16O(7+)
11B
15O(7+)
13C
15N
12C
TOFcorrected
ΔE/ΔX

Fig. 5

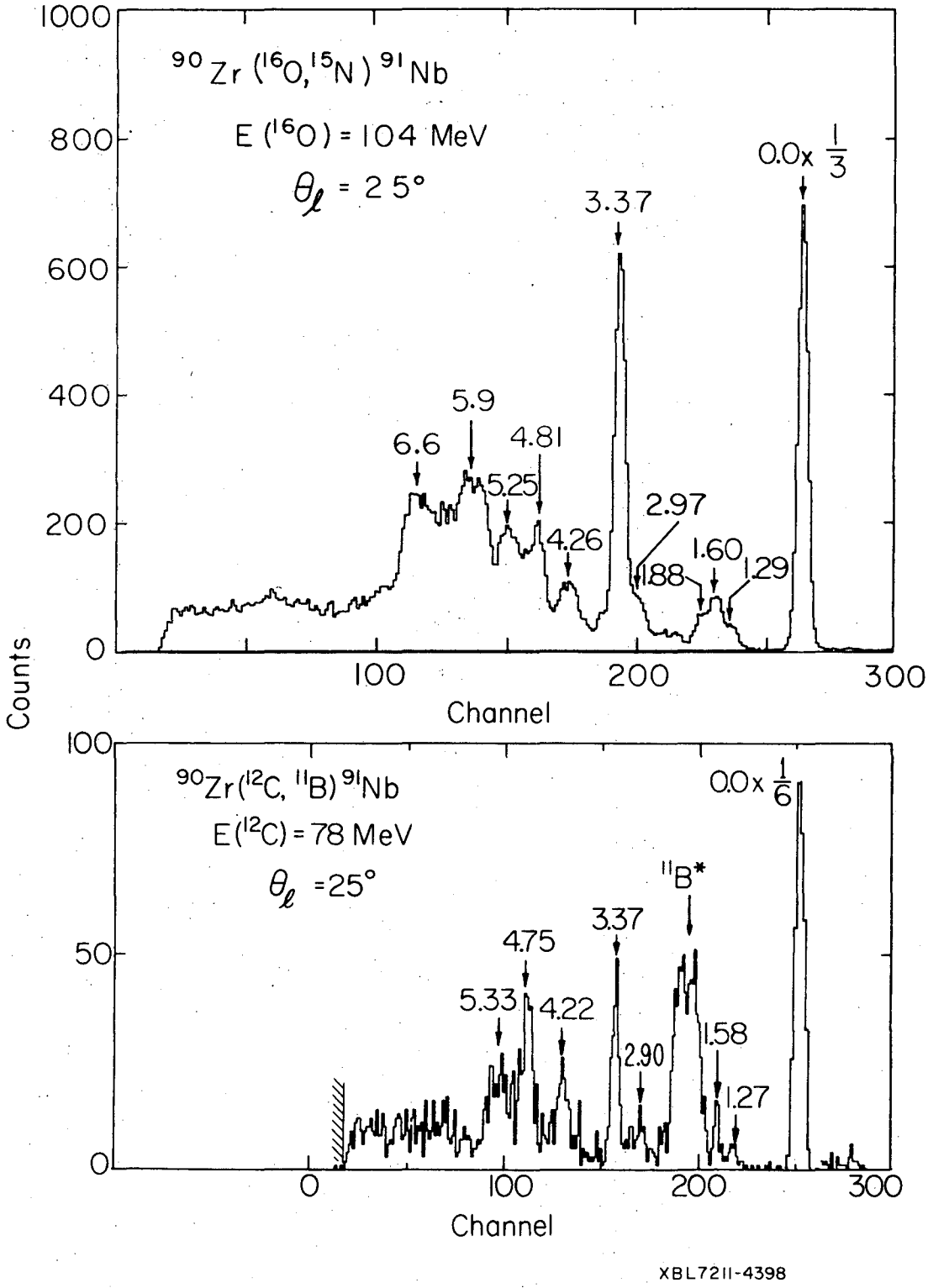
$^{90}Zr(^{16}O,^{15}N)^{91}Nb$
E(^{16}O) = 104 MeV
θ_ℓ = 25°
0.0x 1/3
3.37
5.9
6.6
4.81
5.25
2.97
4.26
1.88
1.60
1.29
Counts
Channel
$^{90}Zr(^{12}C,^{11}B)^{91}Nb$
E(^{12}C) = 78 MeV
θ_ℓ = 25°
0.0x 1/6
$^{11}B^*$
3.37
4.75
5.33
4.22
2.90
1.58
1.27
Channel
XBL7211-4398

Fig. 6

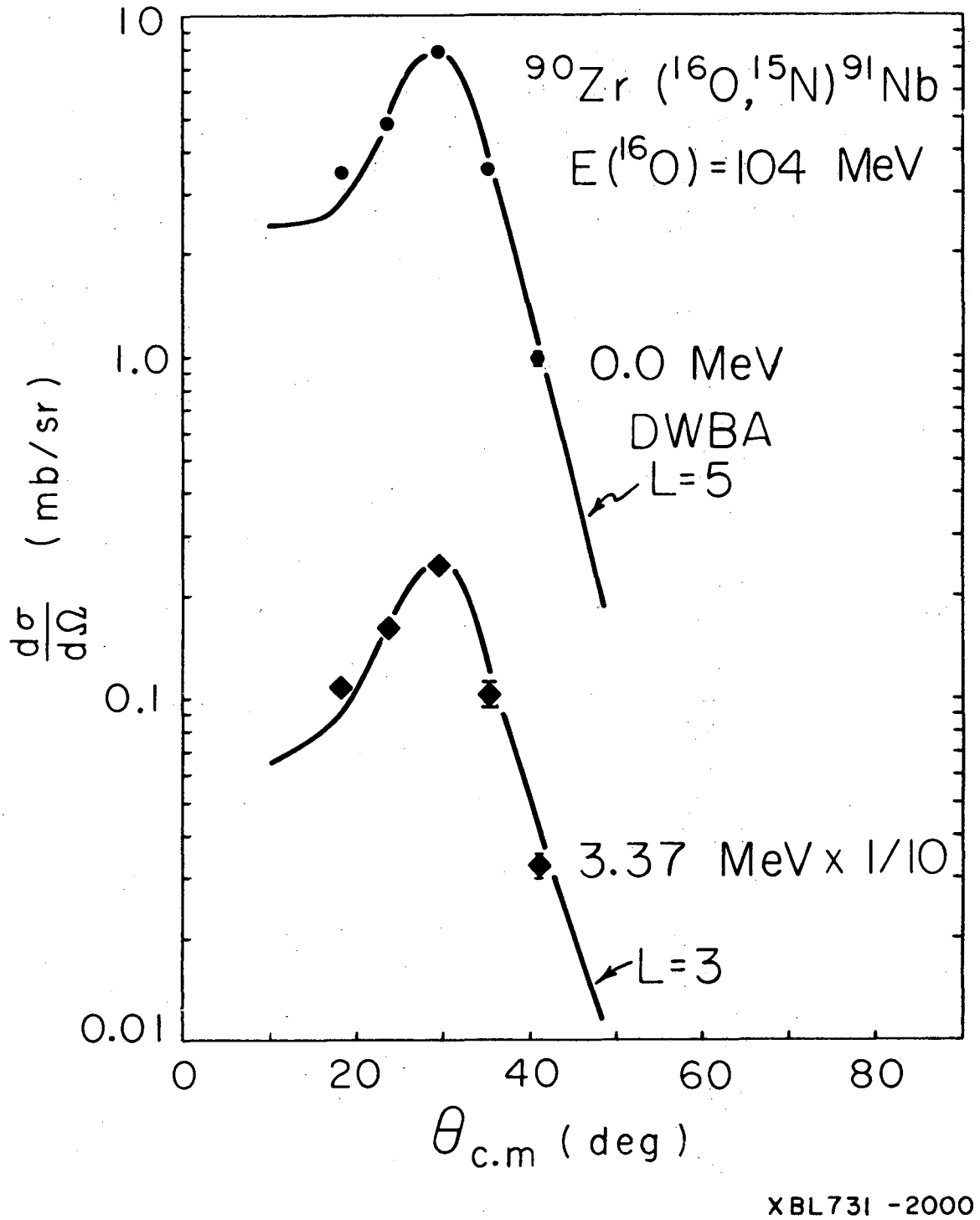
10
1.0
0.1
0.01
$\frac{d\sigma}{d\Omega}$ (mb/sr)
^{90}Zr (^{16}O,^{15}N)^{91}Nb
E(^{16}O) = 104 MeV
0.0 MeV
DWBA
L=5
3.37 MeV x 1/10
L=3
0
20
40
60
80
$\theta_{c.m}$ (deg)
XBL731-2000

Fig. 7

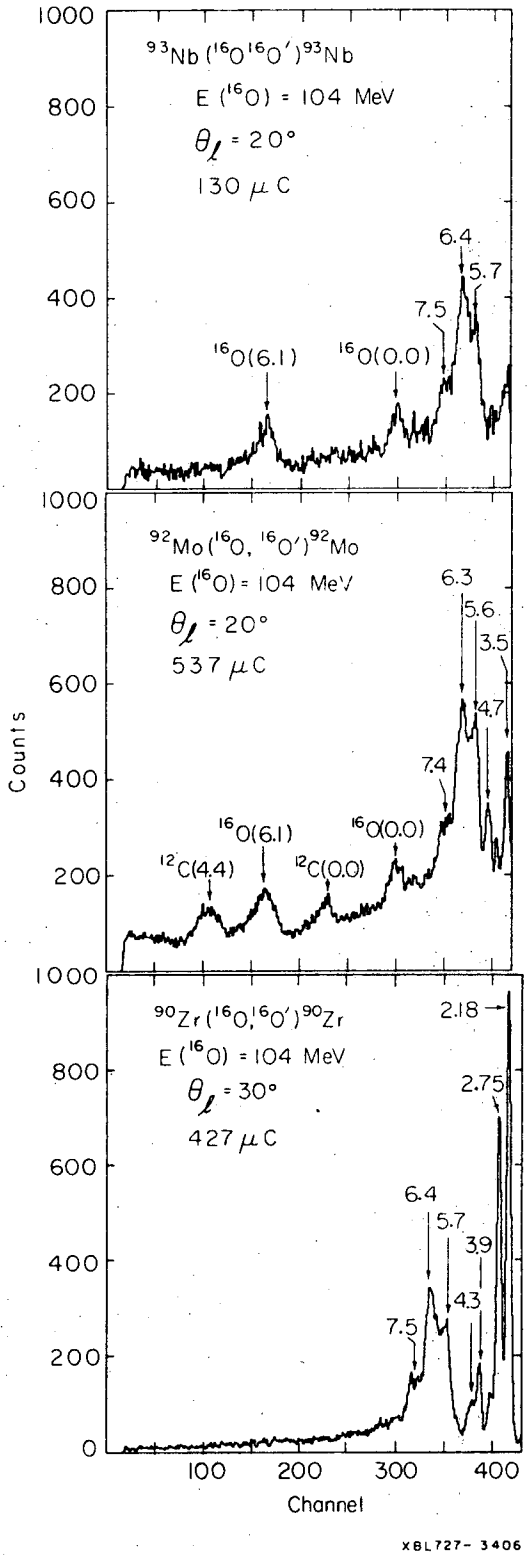
^{93}Nb(^{16}O,^{16}O′)^{93}Nb
E(^{16}O) = 104 MeV
θ_ℓ = 20°
130 μC
^{16}O(6.1)
^{16}O(0.0)
6.4
5.7
7.5
^{92}Mo(^{16}O, ^{16}O′)^{92}Mo
E(^{16}O) = 104 MeV
θ_ℓ = 20°
537 μC
^{12}C(4.4)
^{16}O(6.1)
^{12}C(0.0)
^{16}O(0.0)
6.3
5.6
3.5
4.7
7.4
^{90}Zr(^{16}O,^{16}O′)^{90}Zr
E(^{16}O) = 104 MeV
θ_ℓ = 30°
427 μC
2.18
2.75
6.4
5.7
3.9
4.3
7.5
Counts
Channel
XBL727-3406

Fig. 8

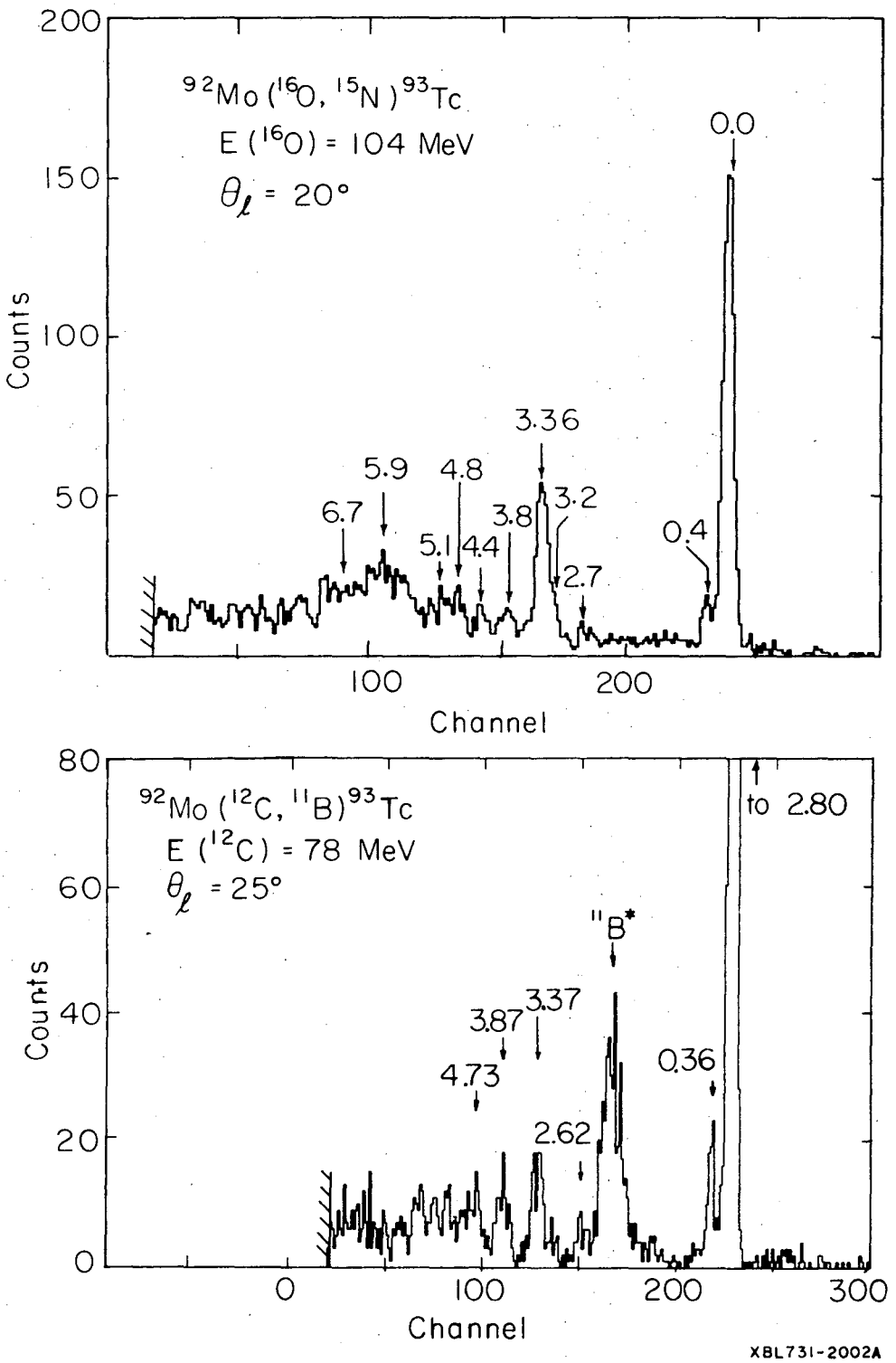
^{92}Mo (^{16}O, ^{15}N) ^{93}Tc
E (^{16}O) = 104 MeV
θ_ℓ = 20°
0.0
0.4
2.7
3.2
3.36
3.8
4.4
4.8
5.1
5.9
6.7
Counts
Channel
^{92}Mo (^{12}C, ^{11}B) ^{93}Tc
E (^{12}C) = 78 MeV
θ_ℓ = 25°
to 2.80
^{11}B*
0.36
2.62
3.37
3.87
4.73
Counts
Channel
XBL731-2002A

Fig. 9

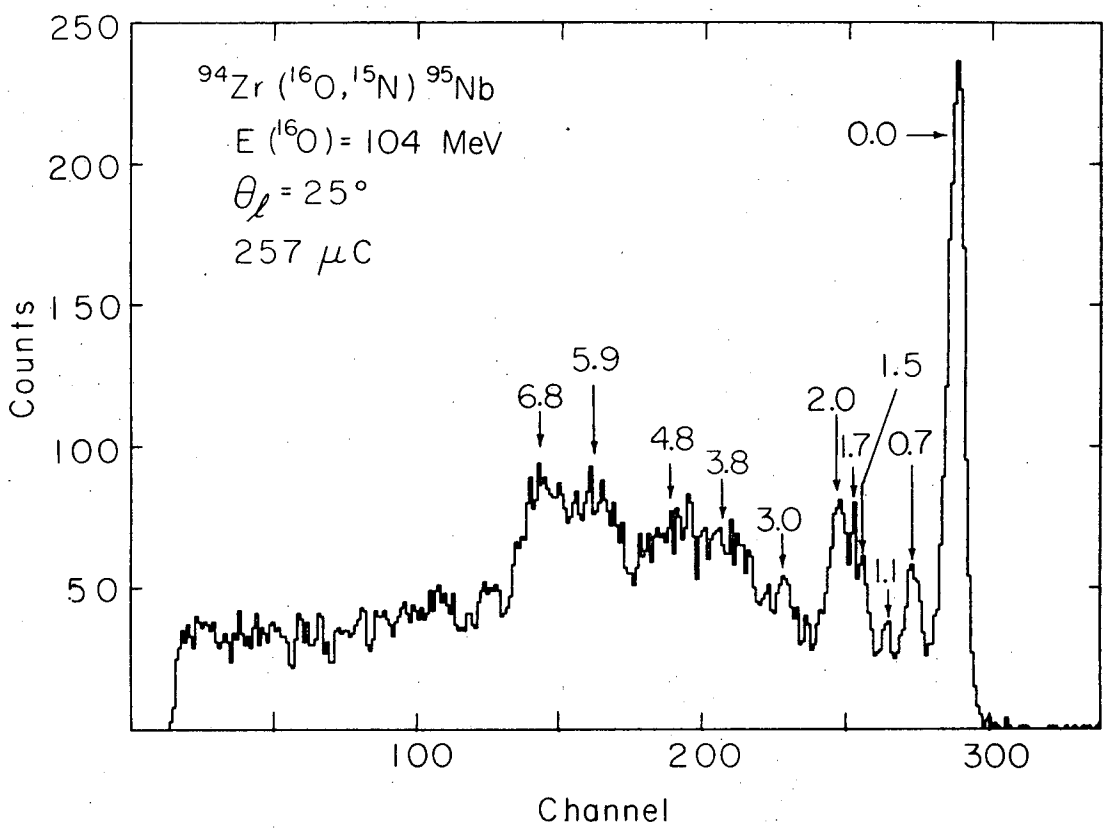
^{94}Zr (^{16}O,^{15}N) ^{95}Nb
E (^{16}O) = 104 MeV
θ_ℓ = 25°
257 μC
0.0
1.5
5.9
6.8
2.0
4.8
1.7
0.7
3.8
3.0
1.1
Counts
250
200
150
100
50
100
200
300
Channel
XBL727 -3442

Fig. 10

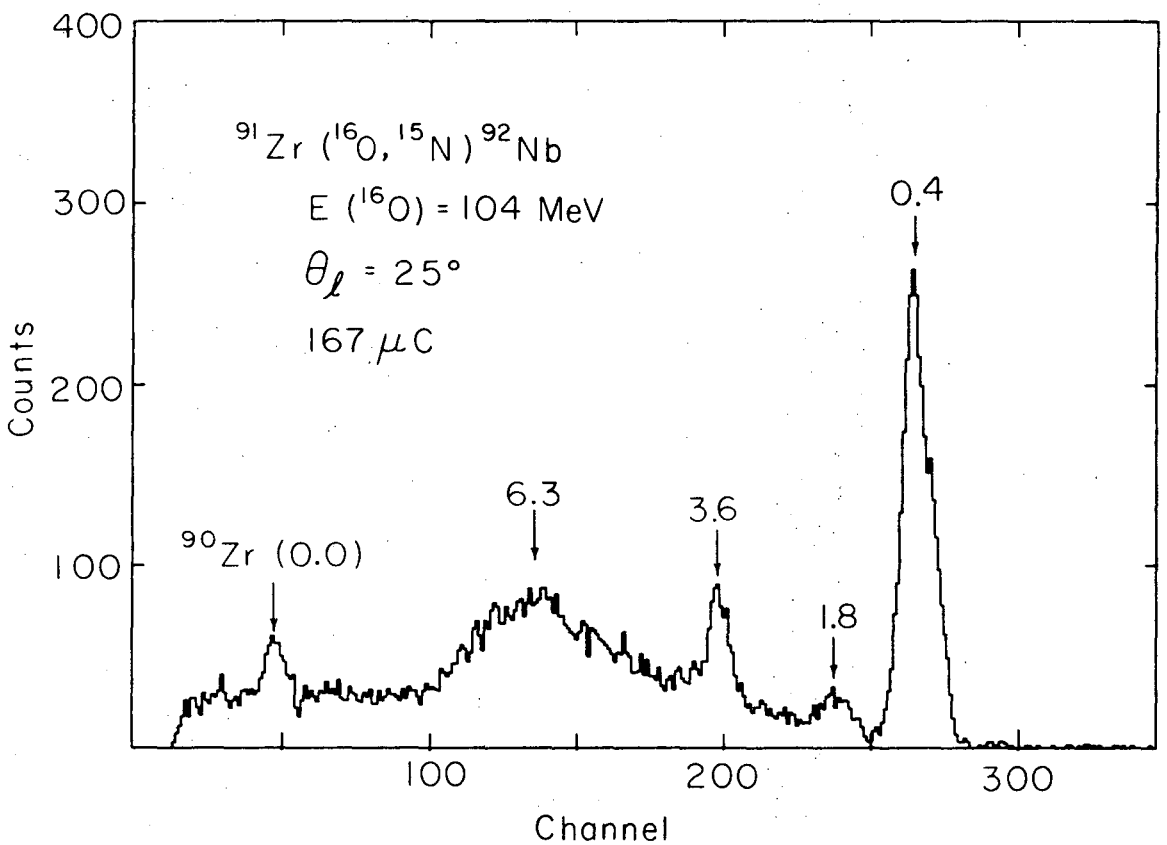
400
300
200
100
Counts
^{91}Zr (^{16}O, ^{15}N) ^{92}Nb
E (^{16}O) = 104 MeV
θ_ℓ = 25°
167 μC
0.4
6.3
3.6
1.8
^{90}Zr (0.0)
100
200
300
Channel
XBL 727-3441

Fig. 11

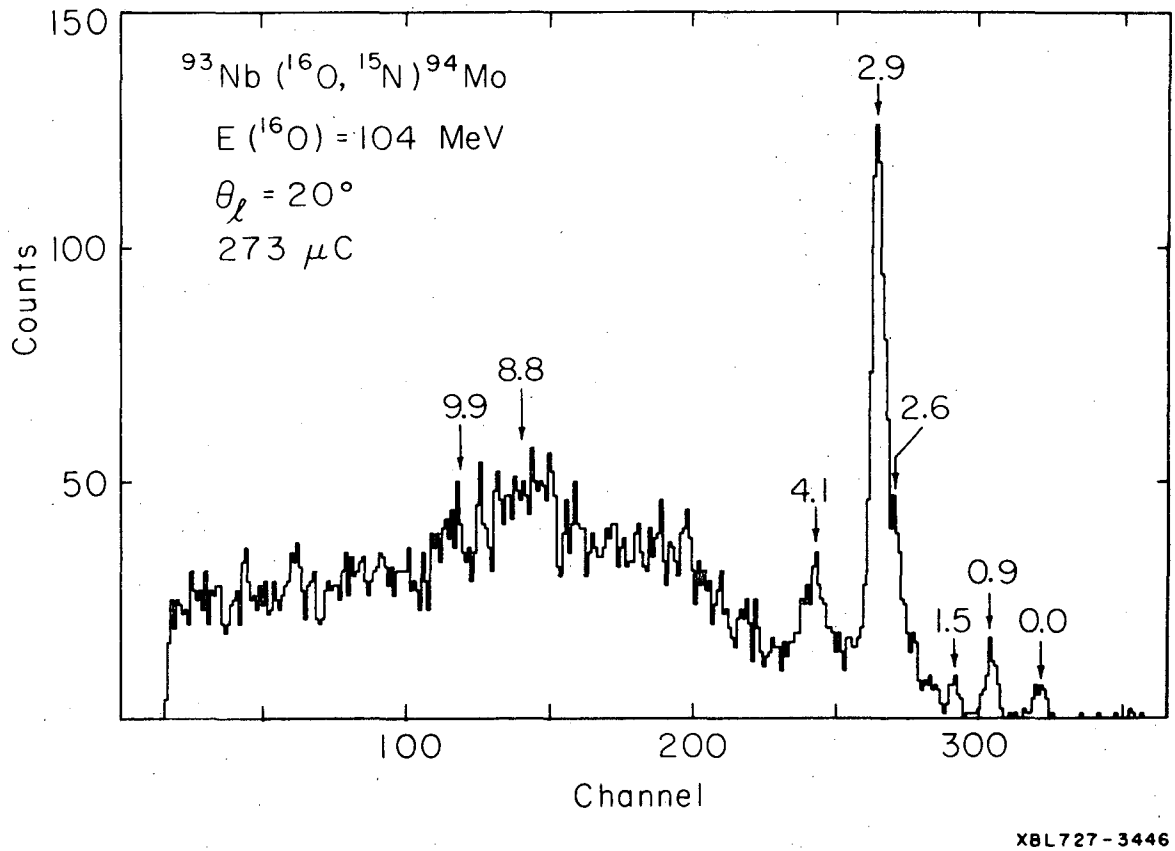
150
100
50
Counts
^{93}Nb (^{16}O, ^{15}N)^{94}Mo
E (^{16}O) = 104 MeV
θ_ℓ = 20°
273 μC
2.9
8.8
9.9
2.6
4.1
0.9
1.5
0.0
100
200
300
Channel
XBL727-3446

Fig. 12

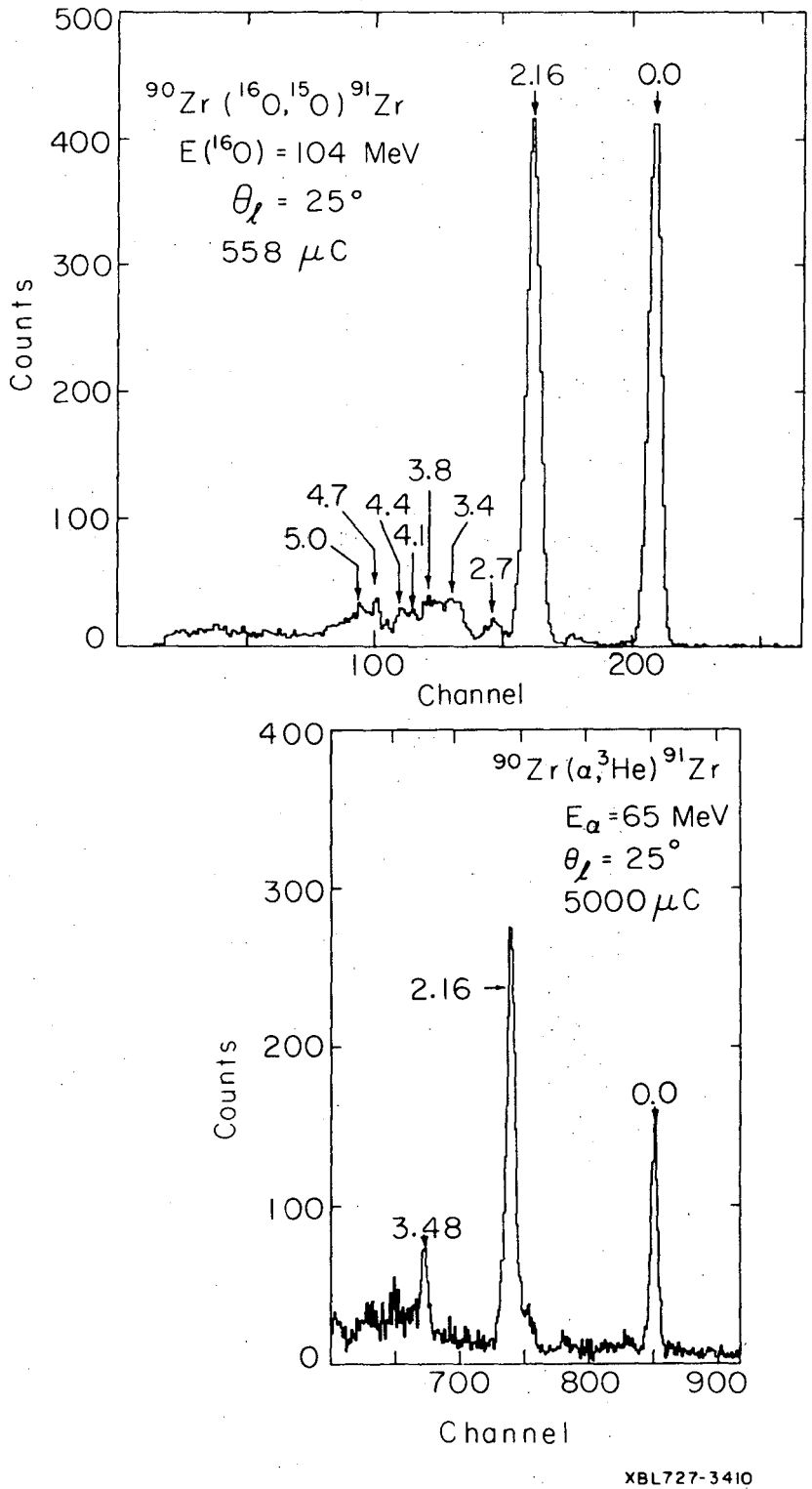
$^{90}Zr\,(^{16}O,^{15}O)\,^{91}Zr$
E(^{16}O) = 104 MeV
θ_ℓ = 25°
558 μC
2.16
0.0
3.8
4.7
4.4
3.4
4.1
5.0
2.7
Counts
Channel
$^{90}Zr(\alpha,^{3}He)\,^{91}Zr$
E_α = 65 MeV
θ_ℓ = 25°
5000 μC
2.16
0.0
3.48
Counts
Channel
XBL727-3410

Fig. 13

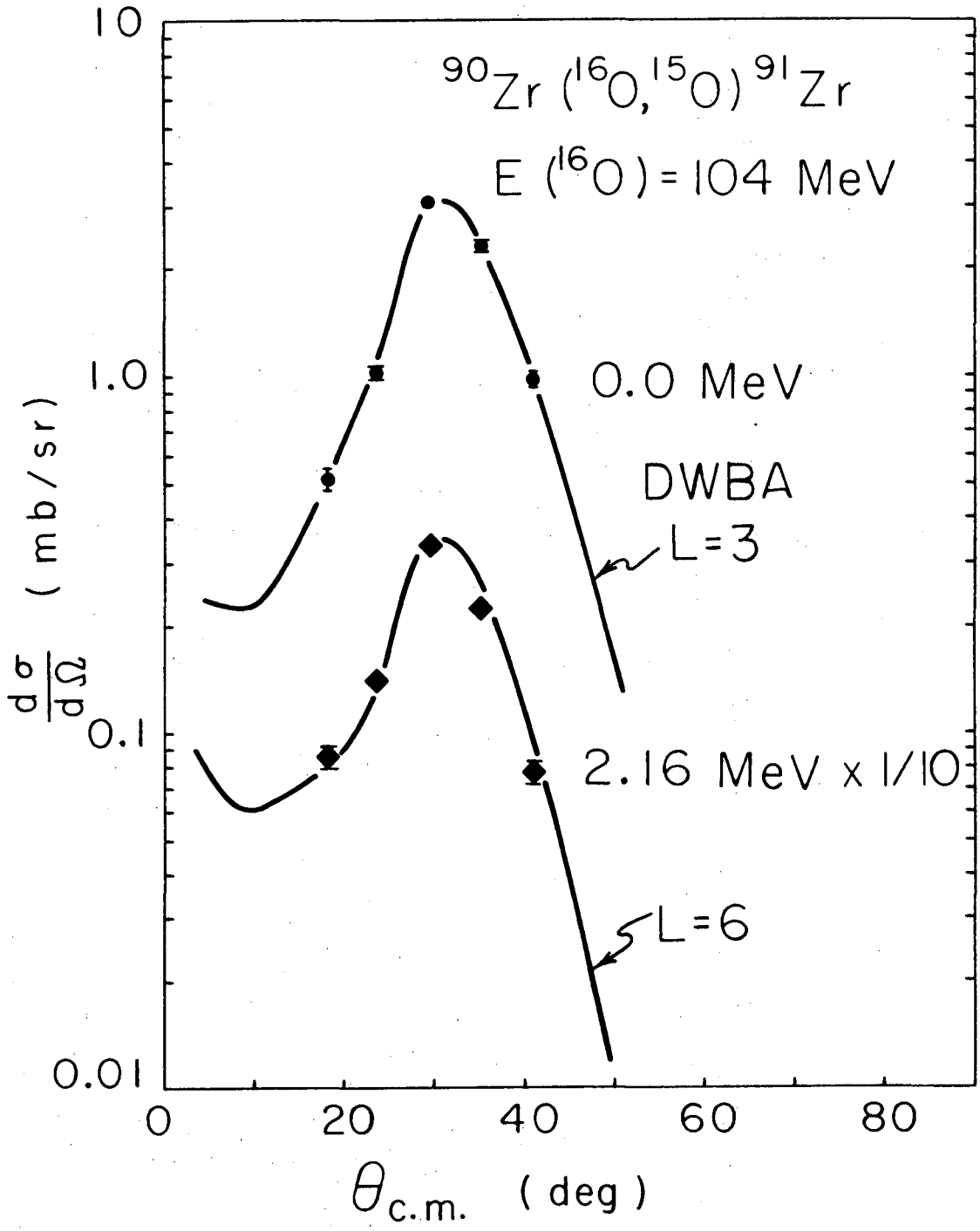

XBL731-2001

Fig. 14

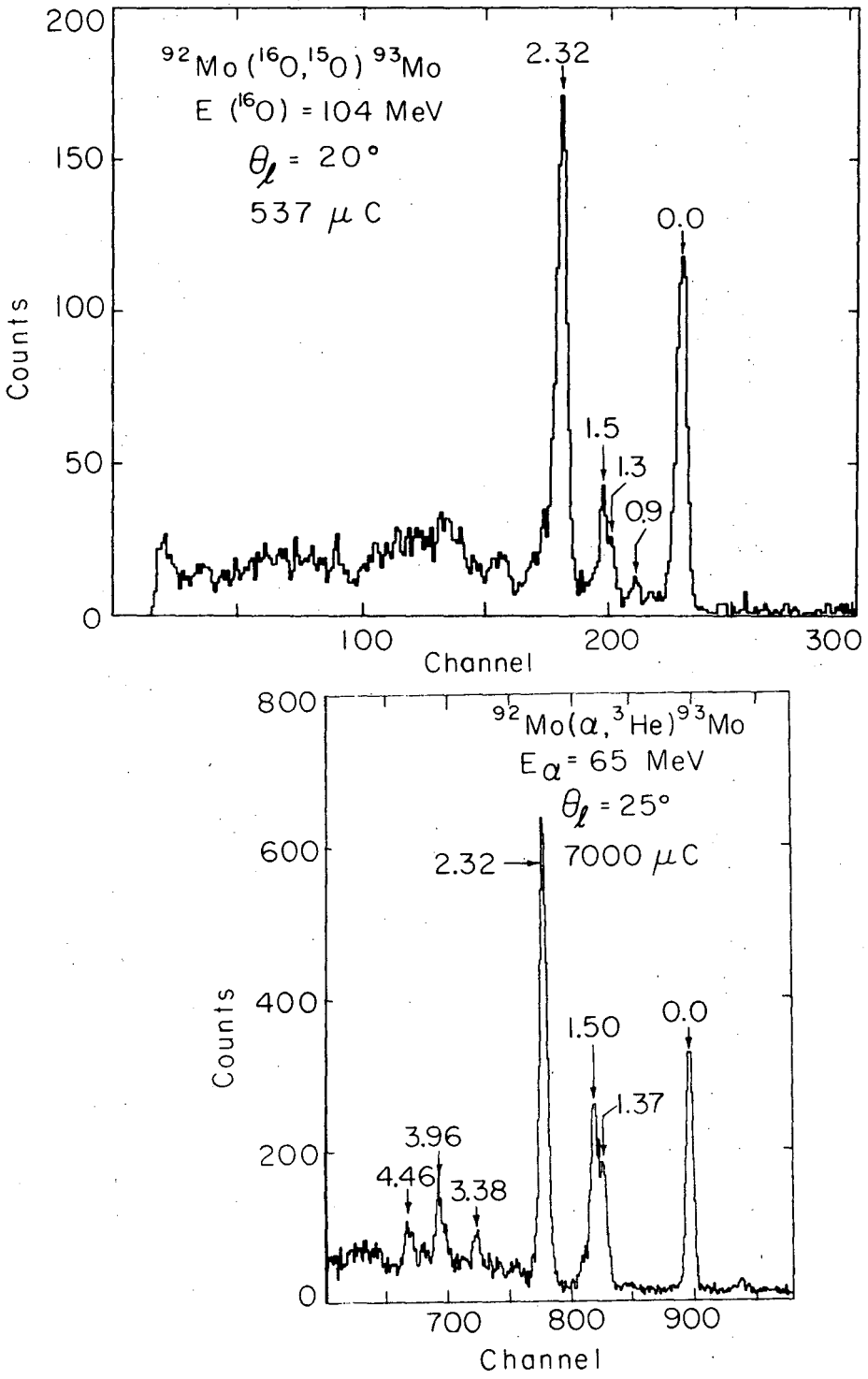

XBL727-3412

Fig. 15

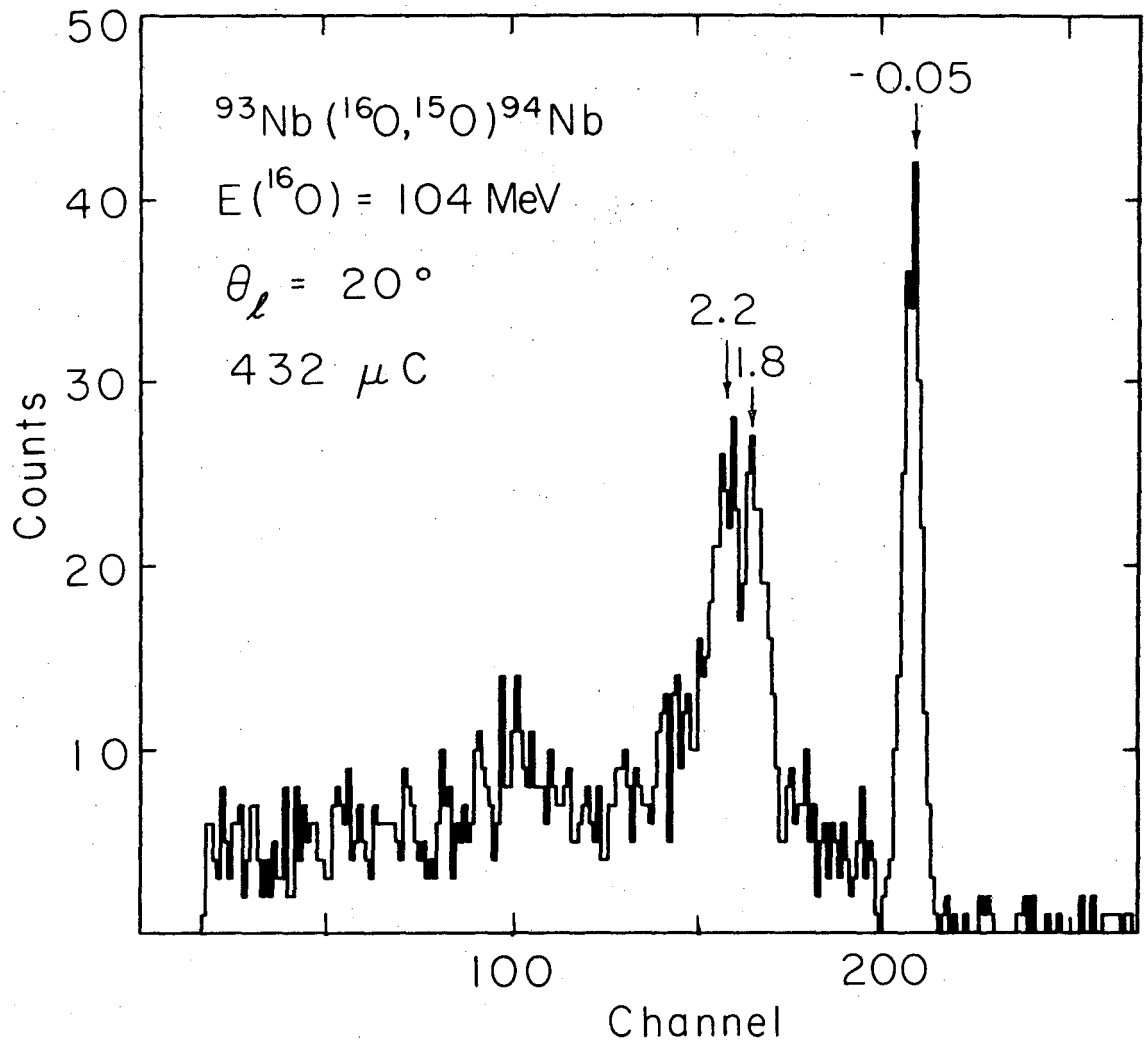
^{93}Nb (^{16}O,^{15}O)^{94}Nb
E(^{16}O) = 104 MeV
θ_ℓ = 20°
432 μC
-0.05
2.2
1.8
Counts
Channel
50
40
30
20
10
100
200
XBL727-3445

Fig. 16

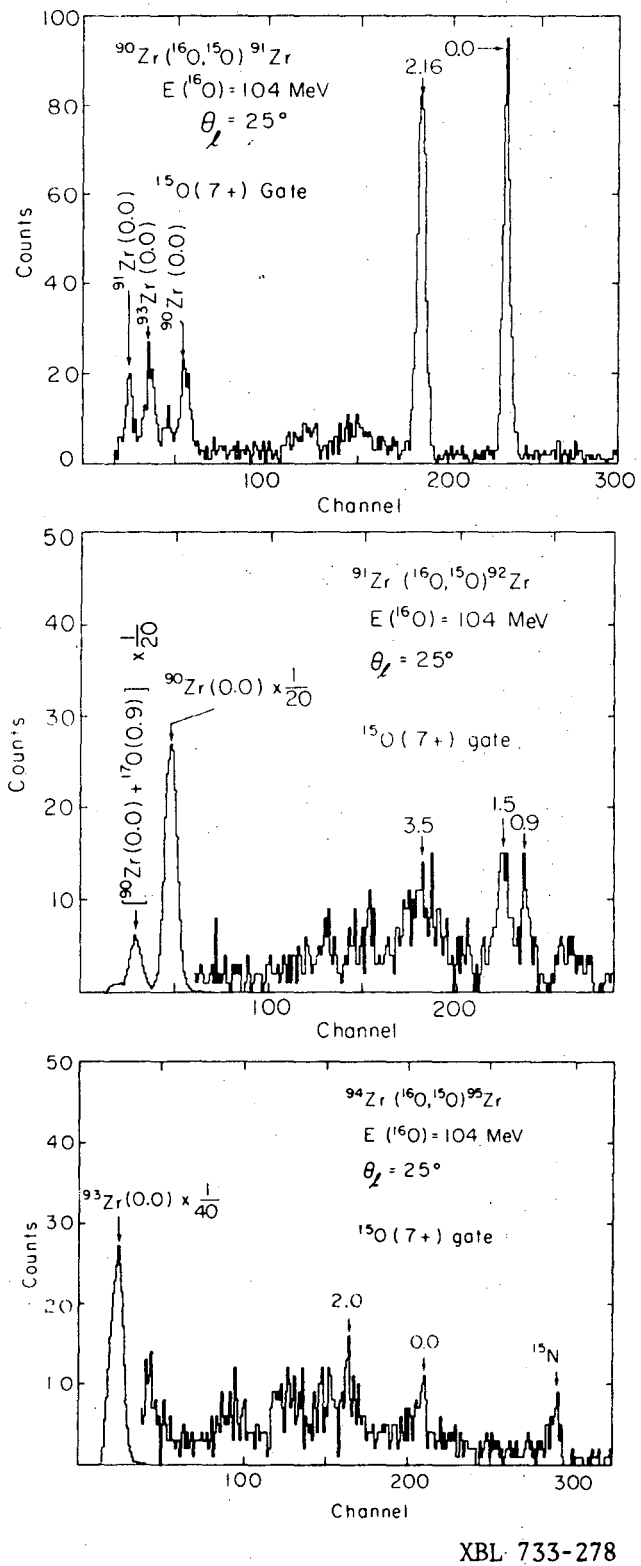

XBL 733-278

Fig. 17

TECHNICAL INFORMATION DIVISION
LAWRENCE BERKELEY LABORATORY
UNIVERSITY OF CALIFORNIA
BERKELEY, CALIFORNIA 94720